accumulation at the top of the column is more, and ranges up to 30mm in comparison to the increasing gas velocity mode. The solids concentration again does not have any appreciable influence except at 523K for 40 weight percent where the foam height decreases dramatically to 100-120mm.

For gas velocities beyond 80 mm/s, the bubbling behavior is the same but the foaming characteristic changes. For decreasing gas velocity, the foam height at the top of the dispersion is negligibly small while for increasing gas velocity the foam heights up to 20 mm are observed. The accumulated foam at the top gets dissipated and distributed in the main body of the dispersion. These remarks are based from the experiments conducted at 473K and 40 weight percent slurry concentration only. The decreasing velocity mode of operation, however, did confirm the above observations, even at 428 and 523K, i.e. no foam formation. The nitrogen gas holdup data for the three-phase system are given in Table 4.25.

4.6 Heat Transfer Data for Large Column

Experimental heat transfer studies were conducted in the 0.305 m diameter bubble column in semi-batch mode for two- and three-phase systems at ambient pressure and in the temperature range 290 to 523K. The heat transfer surfaces employed included a 19 mm diameter tube, a five-, a seven- and a thirty-seven tube bundle. The variation of heat transfer coefficient with height above the distributor plate and along radial distances are also established.

4.6.1 Operating Mode and a Typical Procedure

To establish a methodology for determining T_c the radial temperature profiles are measured at various air velocities for the middle region when the probe is located 160.5 cm above the distributor plate. The results are graphically presented in Fig. 4.60 for four typical air velocities. It is clear that the radial temperature profile is flat and a good estimate of T_c values is possible within an uncertainty of about $\pm$ 0.003K. T_s is obtained by averaging all the six temperatures and these T_s values have a standard deviation of about 0.7. The

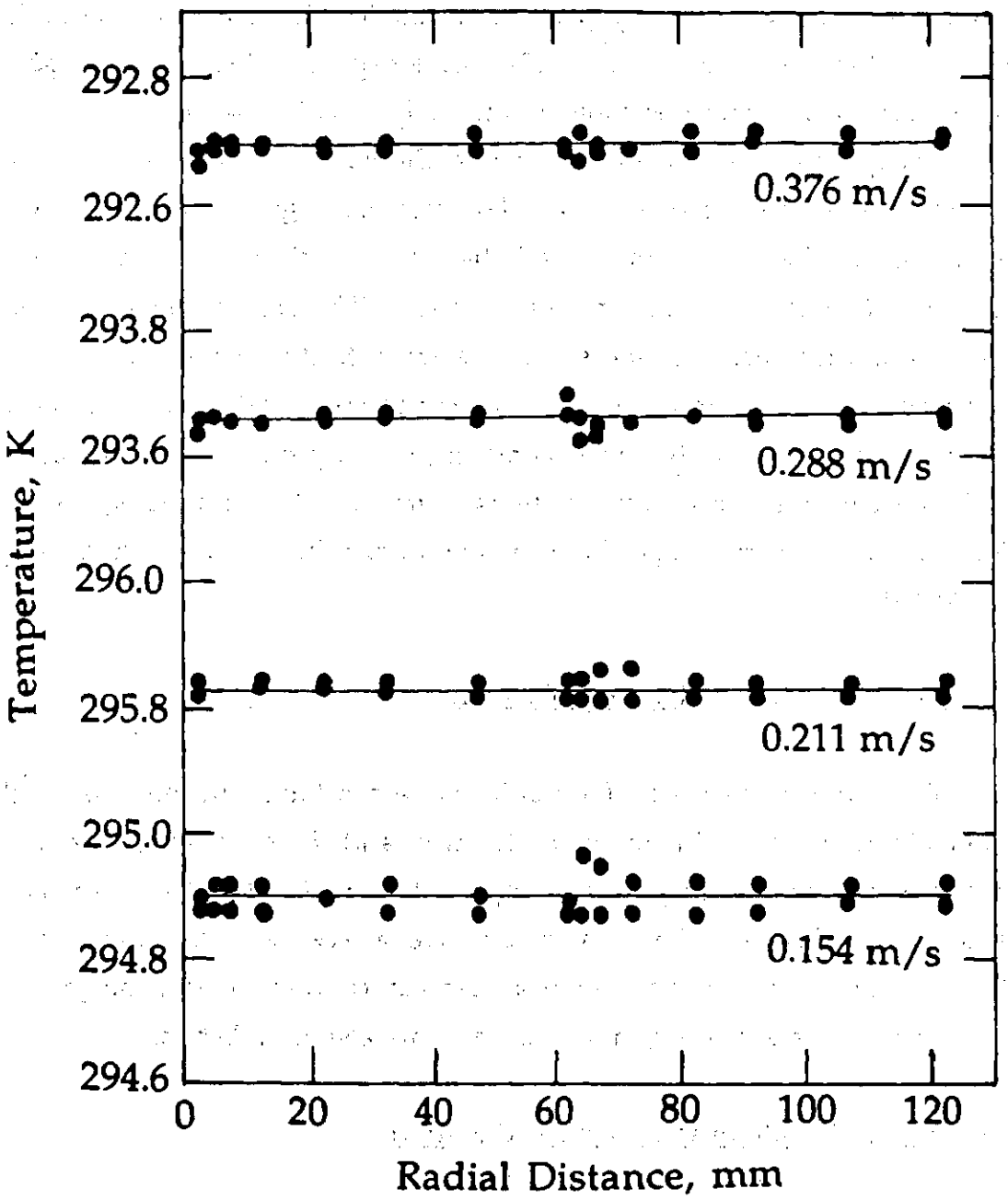

Fig. 4.60. Radial temperature profile at various air velocities.

difference between the maximum and minimum temperatures is always less than about 2K. A is equal to 0.02153 m^2.

The dependence of h_w on the thermal flux (Q/A) is investigated by choosing four values of Q in the range 549.0 - 748.6 W. Computed h_w values are listed in Table 4.29 with other relevant details. T_c is determined by averaging the eight temperatures recorded by the temperature measuring probe located 10 mm away from the heat transfer probe surface. It is inferred from these T_c values that it is not dependent on Q as the scatter is always less than the estimated uncertainty of $\pm$ 4.5%. In all subsequent measurements Q is kept at around 750W.

The heater probes (Fig. 3.17) provide the necessary thermal energy to heat column contents to the desired temperature. At a given gas velocity and temperature, ten instantaneous h_w values are measured in line and h_w is taken to be the mean of these ten values.

4.6.2 Air-Water-System

With the heater located in the lower, middle and upper regions of the column, h_w is measured as a function of time at various air velocities in the range 2.4 - 3.7 cm/s. In the upper region, the mid-point of the heated test section is located 2.188 m above the distributor plate, while their heights are 1.605 and 0.523 m for the middle and lower regions respectively. The 19 mm diameter heat transfer probe containing these three test sections is axially located in the column. The h_w values computed at every two minutes from the measured T_s and T_c values by the data acquisition system are shown in Fig. 4.61. The column temperature as established by the four thermocouples located along the column height and those by the radial temperature probes is also shown in each case along with the corresponding observed maximum deviation. The column temperature exhibits a slow increase in temperature with the passage of time. The increase is more at lower gas velocities as expected. h_w values, in general, are found to be independent of time in view of the relatively small increase in temperature. The continuous lines in each case are obtained from the data points by the method of least squares. h_w values as obtained from the regression

Table 4.29. Experimental h_W (kW/m^2K) values as a function of power input to the probe at U_g = 0.376 m/s. Column diameter: 0.305 m, Internal: 19 mm single tube, System: Air-water.

Q(W)	T_s(K)	T_c(K)	ΔT(K)	h_W
549.0	295.9	292.2	3.72	6.85
617.5	296.4	292.3	4.03	7.11
680.0	296.8	292.5	4.33	7.29
748.6	297.5	292.6	4.85	7.17

Table 4.30. Experimental h_W (kW/m^2K) values in different regions of the 0.305 m bubble column for air-water system at 297 ± 3K. Internal: 19 mm single tube.

Region	Lower	Middle	Upper	Mean
U_g				
0.376	6.954	6.942	7.810	7.23 ± 0.48
0.346	7.018	7.125	7.505	7.22 ± 0.26
0.307	6.825	6.994	7.651	7.15 ± 0.52
0.269	6.795	6.992	7.362	7.00 ± 0.35
0.239	6.611	6.809	7.100	6.84 ± 0.23
0.192	6.493	6.618	6.702	6.60 ± 0.10
0.154	6.071	6.404	6.692	6.38 ± 0.30
0.125		6.289		
0.117	5.995		6.191	6.12 ± 0.16
0.077	6.254		5.843	5.90 ± 0.29
0.048	6.411		5.103	5.68 ± 0.68
0.024	6.152		4.195	5.20 ± 0.98

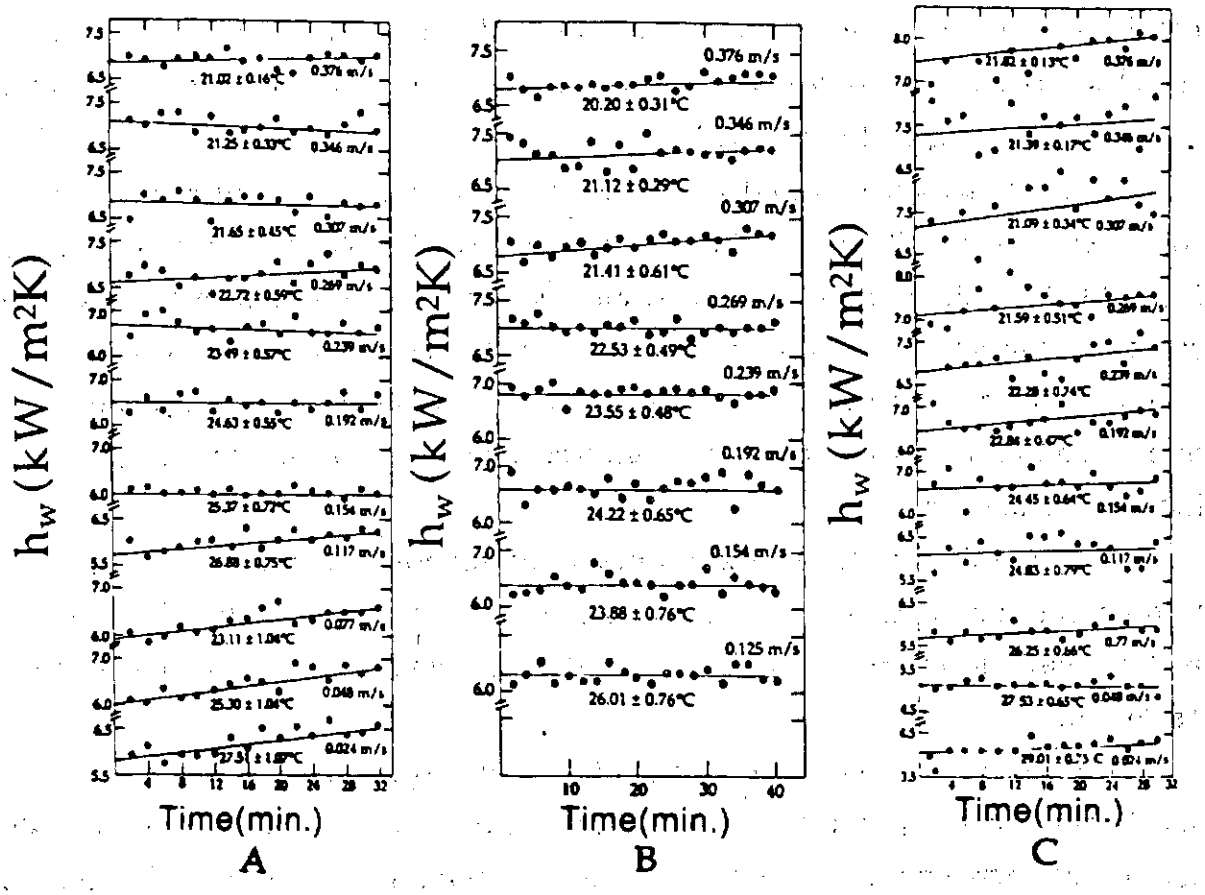

Fig. 4.61. Variation of heat transfer coefficient with time at different air velocities for lower (A), middle (B) and upper (C) regions of the column.

analysis corresponding to the middle of the time interval at each air velocity are listed in Table 4.30 and graphed in Fig. 4.62. An unambiguous dependence of h_w on the position of the test section in the column does not follow from this plot. In view of our estimated uncertainty of about 5% in these values, a mean set is recommended on the basis of all the data points. This set is represented by the continuous lines in each case are obtained from the regression analysis corresponding to the middle of the time interval at each air velocity are listed in Table 4.30 and graphed in Fig. 4.62.

Experimentally measured heat transfer coefficient values from probe P1 of the seven-tube bundle (Fig. 3.17C) as a function of air velocity at temperatures of 303, 313, 323, 333 and 343K for air-water system are presented in Fig. 4.63 and smoothed values are listed in Table 4.31 at round values of air velocities greater than 0.1 m/s at a particular temperature. On the other hand, the dependence is more pronounced and increase is appreciable at a particular velocity with increase in temperature.

Heat transfer coefficient values measured for four different locations in the thirty-seven tube bundle are shown in Fig. 4.64. The data are taken for air-water system with decreasing velocity mode at four temperatures and are given in Table 4.32.

In each case, the heat transfer coefficient is largest for the probe location 3 and lowest for the probe location 1. This would suggest that the heat transfer coefficient increases along with column axis region with increase in column height above the distributor. The comparative dependence of heat transfer coefficient at locations 2 and 4 is somewhat involved and depends primarily on the value of air velocity. At lower air velocities, heat transfer coefficient values at location 2 are smaller than at location 4, but at higher gas velocities the differences are relatively smaller and these are weakly dependent on temperature. At the lowest temperature (298K), position 2 gives slightly higher coefficients and this trend somewhat reverses at the highest temperature (343K). It will be tested on the basis of data where measurements are possible over a wider temperature range. Figure 4.64D, also shows that under similar conditions heat transfer coefficients at position 2 are greater than at position 1.

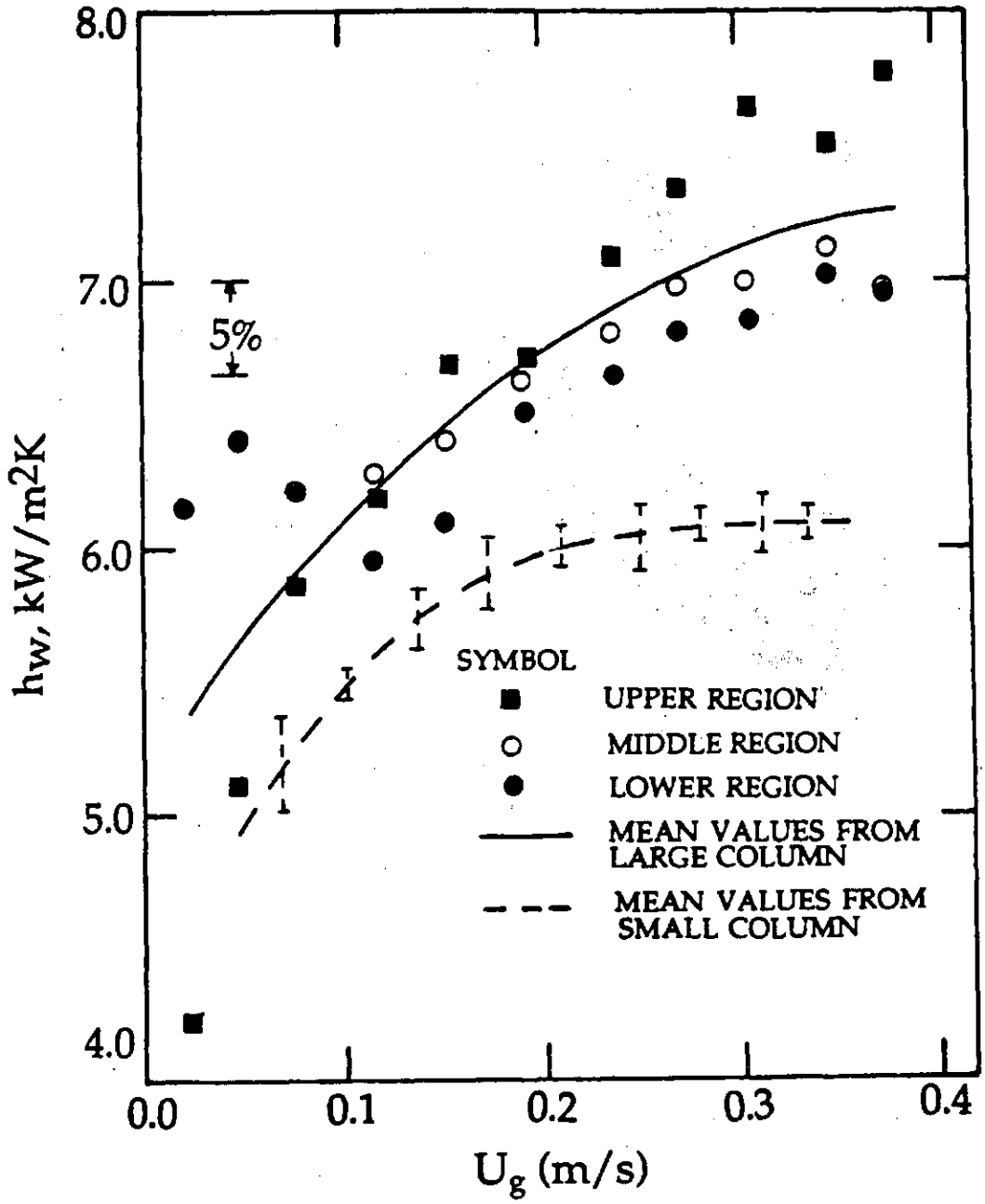

Fig. 4.62. Variaiton of heat transfer coefficient with air velocity for different regions of the column at 297K.

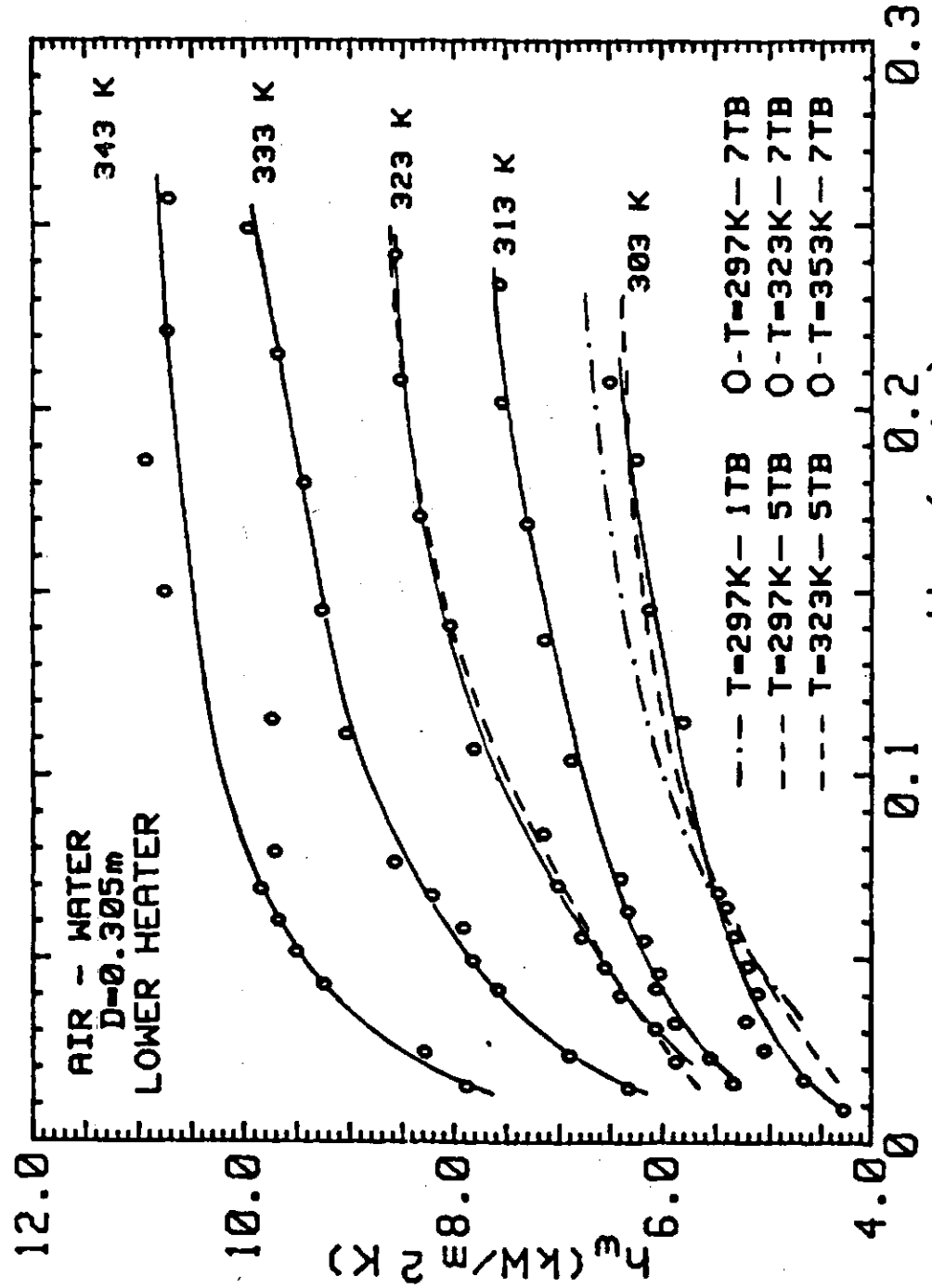

Fig. 4.63. Variation of heat transfer coefficient with temperature, air velocity and tube bundle configuration.

Table 4.31. Smoothed h_W (kW/m^2K) values for air-water system at different temperature levels. Column diameter: 0.305 m, Internal: Seven-tube bundle.

303 K		313 K		323 K		333 K		343 K	
U_g	h_w	U_g	h_w	U_g	h_w	U_g	h_w	U_g	h_w
0.019	4.66	0.018	5.33	0.024	5.86	0.017	6.31	0.017	7.87
0.023	5.04	0.025	5.54	0.033	6.05	0.026	6.89	0.026	8.27
0.031	5.22	0.035	5.87	0.042	6.39	0.044	7.57	0.045	9.24
0.042	5.11	0.044	6.05	0.050	6.54	0.051	7.81	0.054	9.50
0.050	5.20	0.048	6.02	0.058	6.78	0.060	7.90	0.062	9.67
0.058	5.32	0.057	6.16	0.072	7.01	0.069	8.20	0.071	9.84
0.066	5.39	0.065	6.31	0.086	7.14	0.078	8.57	0.081	9.71
0.070	5.46	0.074	6.38	0.109	7.79	0.113	9.03	0.117	9.93
0.116	5.79	0.106	6.87	0.143	8.03	0.147	9.25	0.152	10.75
0.147	6.10	0.139	7.13	0.173	8.32	0.182	9.42	0.188	10.93
0.188	6.22	0.171	7.29	0.210	8.51	0.217	9.68	0.223	10.72
0.209	6.49	0.204	7.53	0.244	8.56	0.251	9.96	0.259	10.71
-	-	0.236	7.55	-	-	-	-	-	-

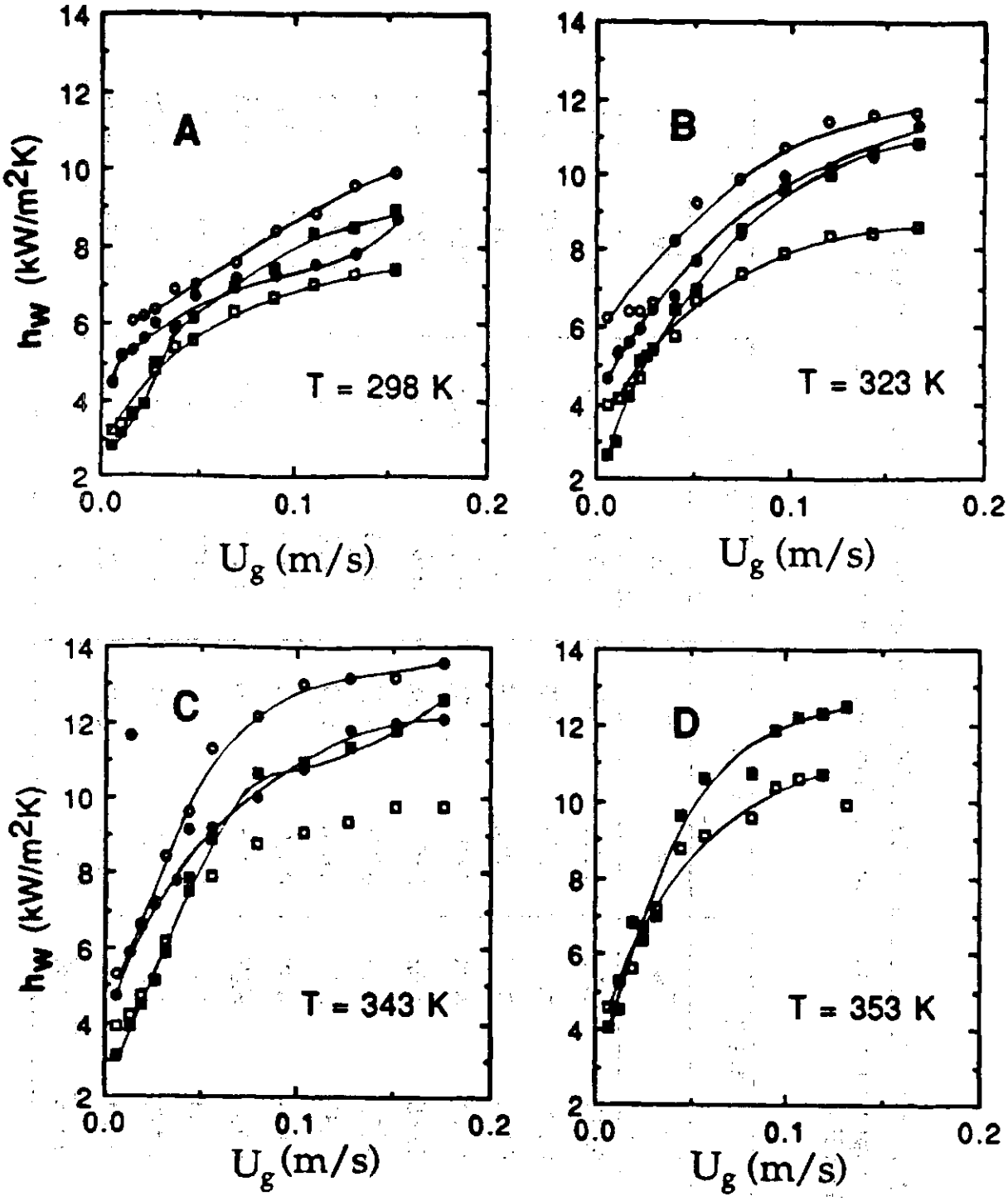

Fig. 4.64. Variation of heat transfer coefficient with decreasing air velocity for air-water system at four locations in the column and at four temperatures. □ Probe 1, ■ Probe 2, ○ Probe 3, ● Probe 4.

Table 4.32. Smoothed h_W (kW/m^{2}K) values for air-water system at different temperature levels in different regions of the tube bundle. Column diameter: 0.305m, Internal: Thirty-seven tube bundle.

U_g	298K				323K				343K				353K	
m/s	Probe 1	Probe 2	Probe 3	Probe 4	Probe 1	Probe 2	Probe 3	Probe 4	Probe 1	Probe 2	Probe 3	Probe 4	Probe1	Probe 2
0.01	3.333	3.333	5.200	4.933	4.000	3.000	5.333	5.167	4.000	3.333	5.933	5.333	5.000	4.333
0.02	4.000	4.167	6.133	5.400	4.667	4.667	6.533	5.933	4.667	4.667	6.800	7.000	6.000	5.333
0.04	5.500	6.000	7.000	6.533	6.167	6.667	8.133	7.267	7.200	7.333	9.333	8.667	8.000	8.600
0.06	6.100	6.800	7.333	7.000	7.000	8.000	9.600	8.000	8.000	9.333	11.333	9.333	9.333	10.667
0.08	6.667	7.333	7.933	7.267	7.333	9.000	10.333	9.000	8.667	10.500	12.067	10.100	10.000	11.333
0.10	6.833	7.867	8.667	7.400	7.933	9.867	10.800	9.667	9.000	10.800	12.733	10.667	10.600	12.067
0.12	7.267	8.500	9.000	7.500	8.333	10.133	11.333	10.133	9.267	11.167	13.167	11.333	10.733	12.500
0.14	7.333	8.733	9.500	8.000	9.200	10.667	11.600	10.633	9.400	11.400	13.267	11.833	—	—
0.16	—	—	—		9.333	10.800	11.667	11.000	9.867	11.933	13.333	11.967	—	—
0.18	—	—	—		—	—	—		9.933	—	—	—	—	—

These heat transfer data suggest that in the column, the coefficient increases with height above the distributor and at the same height it also increases with a radial distance from the column axis except in a region very close to the column wall. This is in accordance with the column hydrodynamic picture detailed by us elsewhere. At higher elevations resulting in greater churning of the liquid with increasing height above the gas distributor plate. The liquid circulation is more with increasing radial distance from the column axis where coalesced bubbles rise up the column while the liquid descends in the regions away from the column axis. This motion is perturbed by the probes. Near the column wall liquid motion is feeble as the bubbles have the tendency to move away from the column wall. This explains why heat transfer coefficient increases with the radial distance from the column axis but is somewhat lower in a region close to the column wall.

4.6.3 Nitrogen-Therminol System

Heat transfer coefficients are measured for probes 1 and 3 of the thirty-seven tube bundle at two temperatures and for three values of Q in each case as a function of U_g with the results displayed in Fig. 4.65. It is concluded that h_W is not dependent on heat flux in this range and in our subsequent work we have chosen Q equal to 45W for the two lower temperatures, and 122W for the next four higher temperatures.

In Fig. 4.66, the heat transfer coefficient values measured for the two-probe locations 1 and 3 are presented as a function of gas velocity at several temperatures. These data are employed to investigate the dependence of h_W on the location of the probe in the bundle. From Fig. 4.66, it is clear that h_W values at lower position (P1) are smaller than at higher vertical position (P3) in the nonfoaming regime (Fig. 4.66 a - c). On the other hand, in the foaming regime (Fig. 4.66 d and e) there is an involved dependence of h_W on probe location.

The experimental h_W data for probes 1 and 3 are presented in Fig. 4.67 to highlight the influence of temperature on heat transfer coefficient. In each case an unambiguous increase in the value of h_W with increase in temperature is

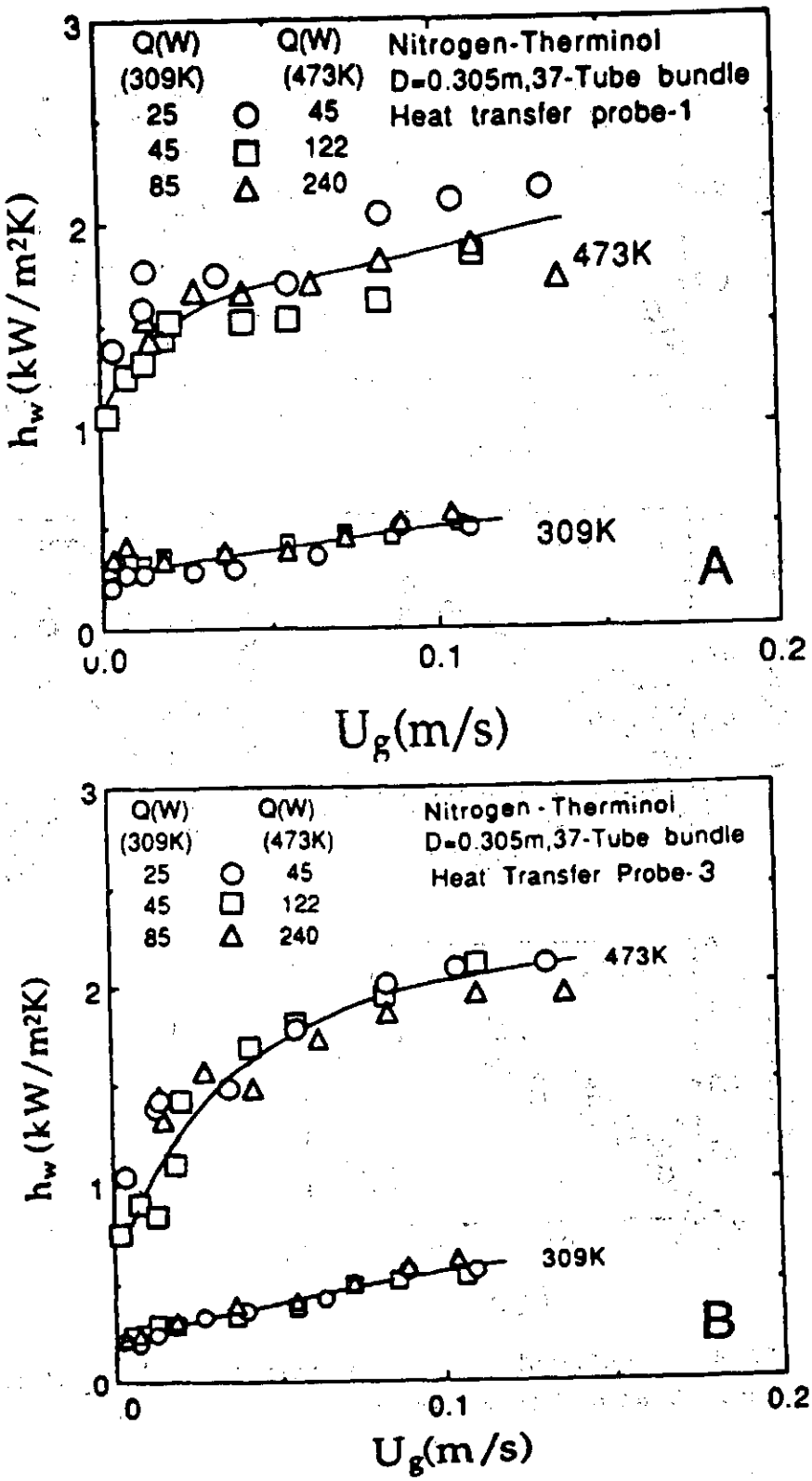

Fig. 4.65. Dependence of heat transfer coefficient on thermal flux as a function of gas velocity and column temperature: (A) probe-1 and (B) probe-3.

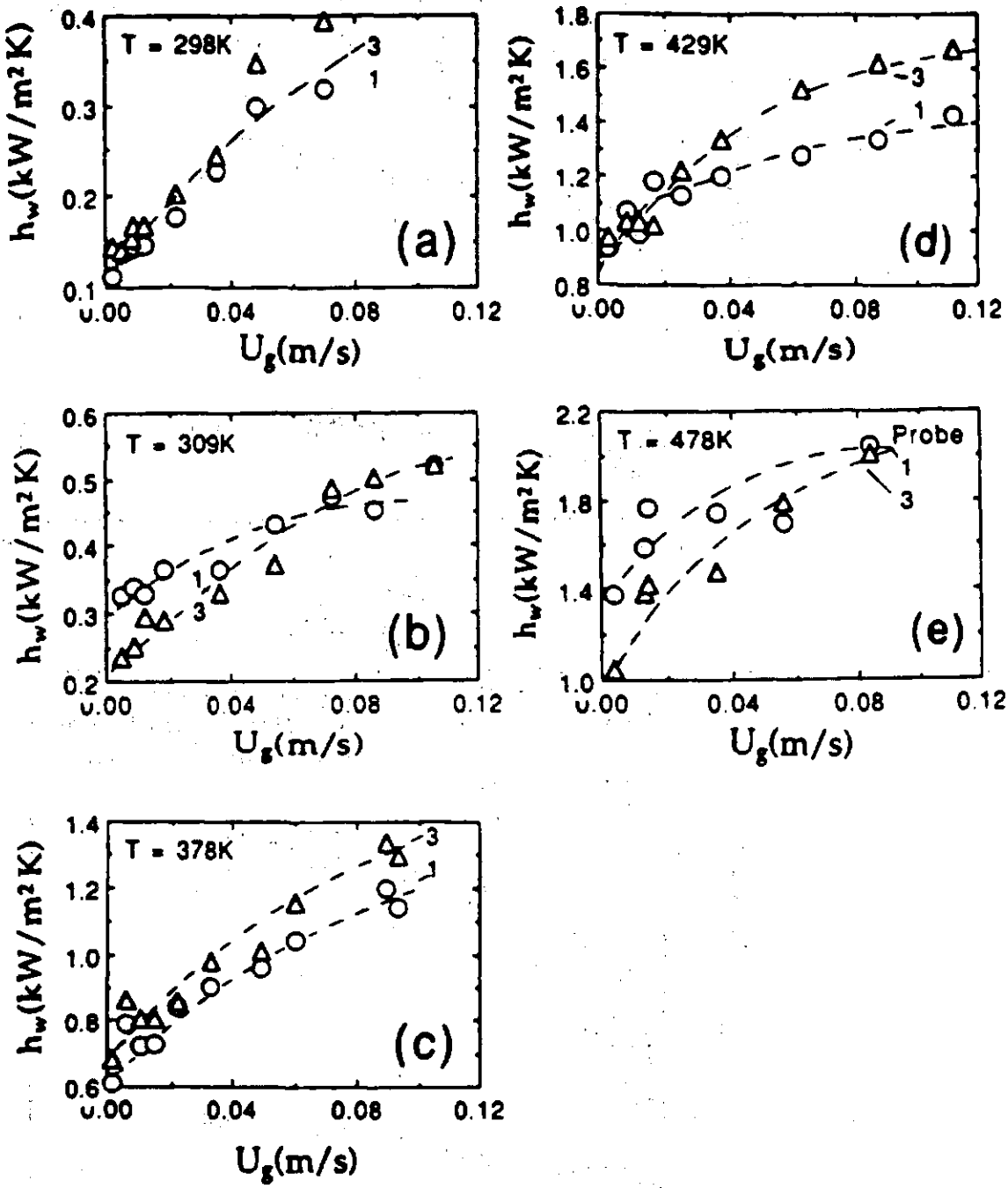

Fig. 4.66. Axial and radial variation of h_W with U_g at different temperatures. Solids Concentration = 0 wt%.

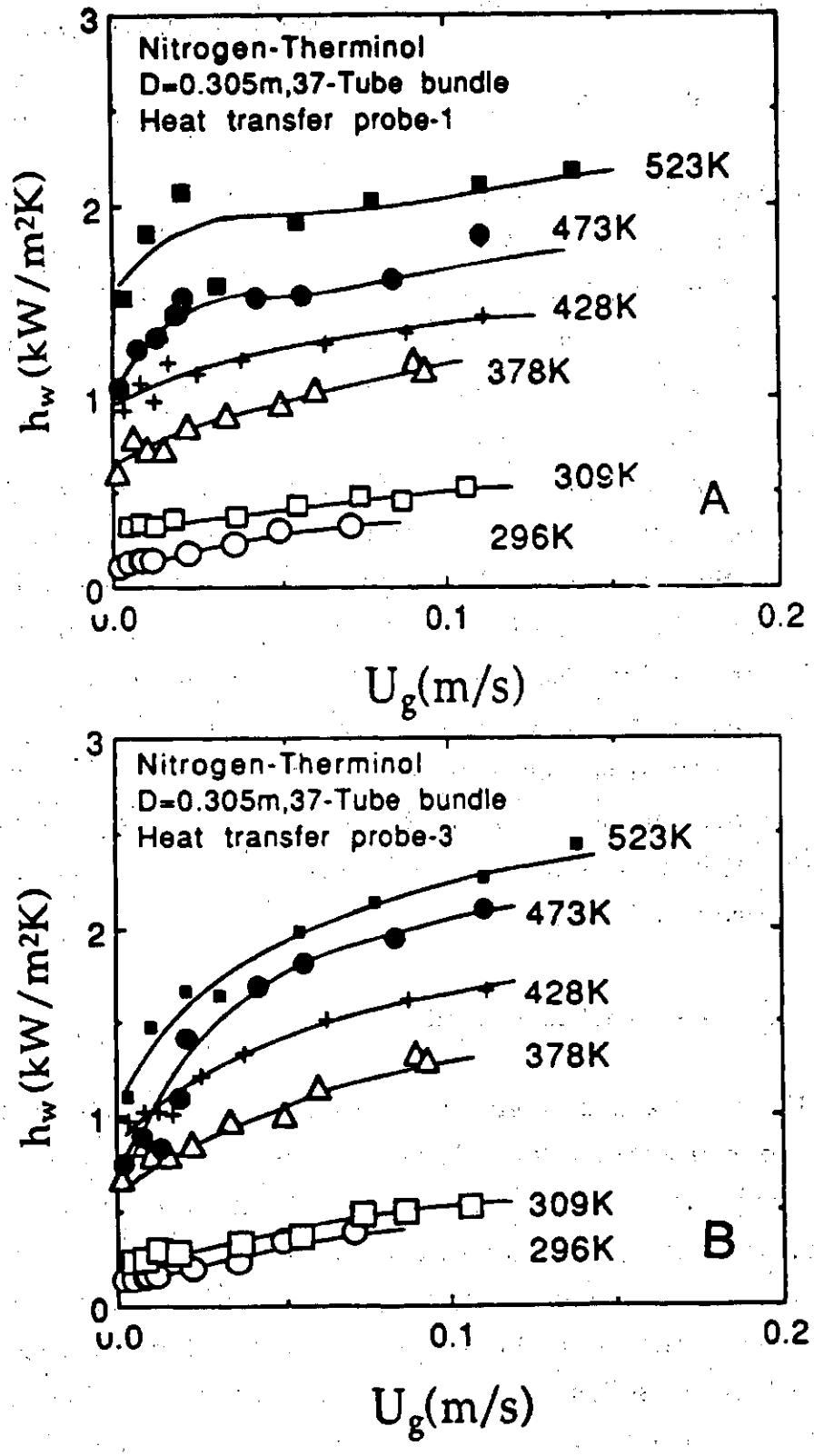

Fig. 4.67. Variation of heat transfer coefficient with gas velocity and temperature for (A) probe-1, and (B) probe-3.

observed. The smoothed h_W values are given in Table 4.33.

4.6.4 Air-Water-Silica Sand System

In Fig. 4.68, the heat transfer data are presented for the air-water-sand system at three temperatures (297, 323 and 343K) and two slurry concentrations as a function of air velocity. The data for air-water system at the same temperatures are also shown for comparison. Again certain trends of practical signficance are obvious. The heat transfer coefficient increases with air velocity but the increase with temperature is much more pronounced. The influence of slurry concentration on heat transfer coefficient is probably more pronounced. The influence of slurry concentration on heat transfer coefficient is probably nominal except in the discrete bubbling regime where it appears to be relatively more pronounced due to the inadequate mixing of the slurry phase at relatively smaller air velocity. The measurements at 323K and for 10 weight percent slurry are considered unreliable and could not be repeated due to malfunction of the column. At lower air velocities, the sand could not be suspended uniformly and it got settled on the air distributor plate and it plugged it partially, and the experiment had to be discontinued. Smooth values of heat transfer coefficient are reported in Table 4.34.

4.6.5. Air-Water-Glass Bead System

The heat-transfer coefficient data for slurry of 143.3 μm average diameter glass beads in water, at three slurry concentrations, are presented in Fig. 4.69A at three temperatures. Also shown in this figure are the air-water system data. Several interesting qualitative trends follow from these plots. In general, the three-phase data follow the same qualitative trends mentioned earlier for the two-phase system. In addition, it may be noted that at a given air velocity and temperature the solids concentration has a negligible influence on heat transfer coefficient. This conclusion is well valid even when the solids concentration is zero. It may be emphasized that the large increase in the observed heat transfer coefficient values with temperature for the air-water system is well substantiated

Table 4.33. Smoothed h_W (kW/m^{2}K) values for nitrogen-Therminol-magnetite system at different temperature levels. Column diameter: 0.305 m, Internal: Thirty-seven tube bundle. Particle diameter: 36.6 μm, Solids concentrations: 0, 15, 30 and 40 wt%.

	T = 298 K				323 K			378 K				428 K				473 K		523 K	
U_g (m/s)	Probe --> 1,2		3,4		1,2		3,4	1,2		3,4		1,2		3,4		1,2	3,4	1,2	3,4
	solids concentration (weight percent) -->																		
	0-30	40	0-30	40	15-30	40	15-40	0-30	40	0-30	40	0-30	40	0-30	40	0-40	0-40	0-40	0-40
0.004	0.125	0.315	0.135	—	—	—	—	0.440	0.650	0.420	0.670	—	—	—	—	—	—	—	—
0.007	0.135	0.332	0.155	—	0.345	0.474	0.355	0.465	0.700	0.480	0.730	0.97	—	0.82	—	1.20	1.00	1.40	1.01
0.010	0.150	0.342	0.170	0.320	0.352	0.490	0.380	0.500	0.720	0.585	0.780	1.02	1.41	0.91	1.14	1.26	1.07	1.43	1.11
0.020	0.190	0.382	0.220	0.365	0.385	0.525	0.432	0.600	0.840	0.680	0.835	1.15	1.45	1.08	1.22	1.39	1.22	1.01	1.37
0.030	0.230	0.415	0.252	0.382	0.415	0.562	0.480	0.680	0.920	0.780	0.880	1.23	1.50	1.18	1.27	1.50	1.35	1.70	1.51
0.040	0.261	0.440	0.282	0.405	0.448	0.592	0.530	0.750	0.990	0.855	0.915	1.29	1.54	1.26	1.31	1.59	1.45	1.93	1.63
0.060	0.330	0.470	0.350	0.442	0.520	0.640	0.620	0.880	1.080	1.010	0.960	1.36	1.58	1.34	1.38	1.70	1.57	2.18	1.81
0.080	0.385	0.500	0.390	0.480	0.605	0.692	0.672	1.010	1.150	1.120	1.010	1.41	1.44	1.43	1.43	1.75	1.67	2.33	1.97
0.090	0.410	0.508	0.410	0.500	0.635	0.710	0.685	1.060	1.180	1.100	1.160	1.44	1.51	1.45	1.44	1.81	1.71	2.41	2.04
0.100	—	—	—	—	—	—	—	1.100	1.200	1.200	1.000	1.46	1.52	1.47	1.46	1.83	1.72	2.50	2.10
0.120	—	—	—	—	—	—	—	—	—	—	—	1.48	1.56	1.51	1.44	1.90	1.76	2.57	2.20
0.140	—	—	—	—	—	—	—	—	—	—	—	—	—	—	—	1.92	1.74	2.51	2.28

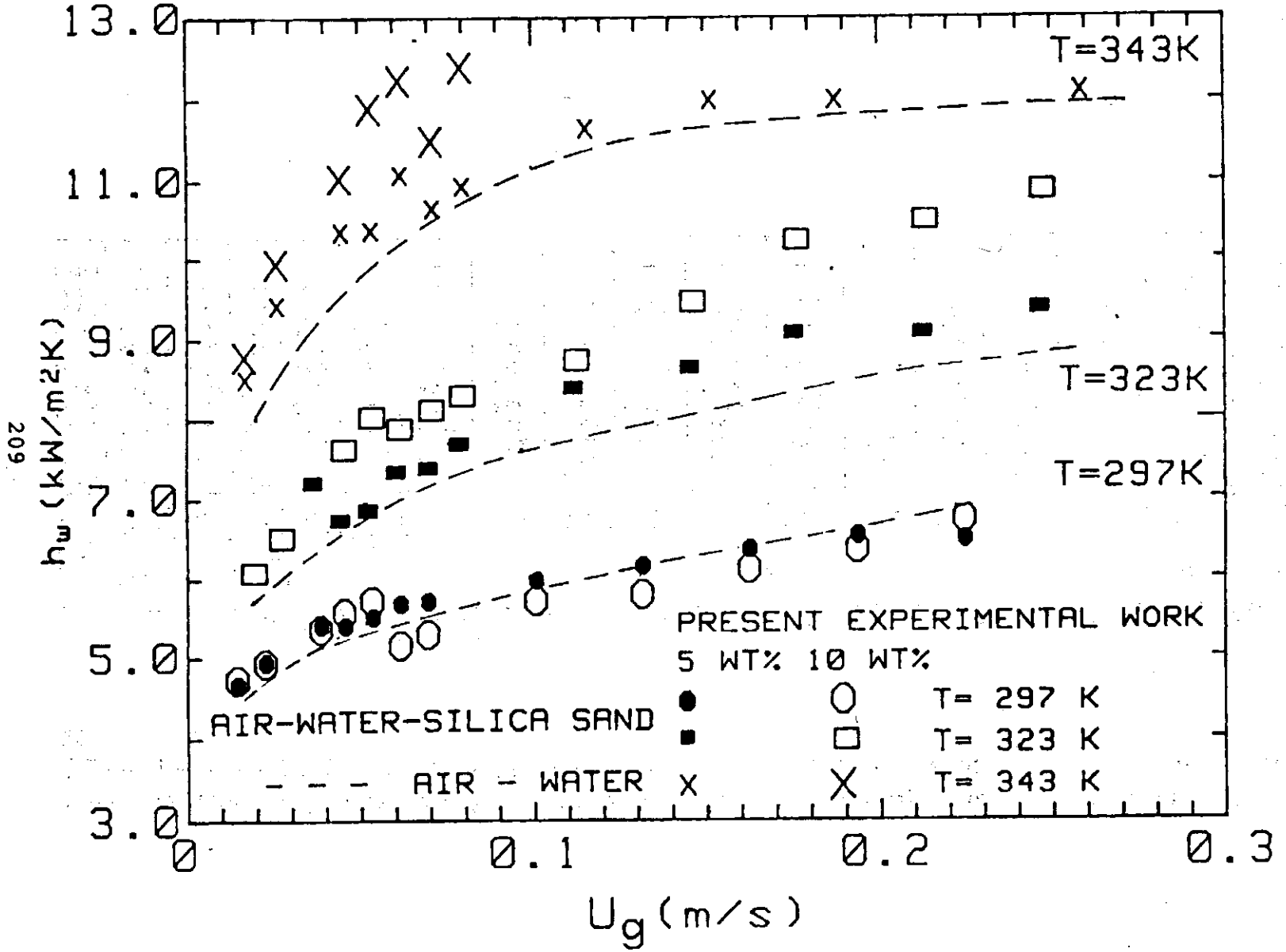

Fig. 4.68. Variation of heat transfer coefficient with air velocity, temperature and slurry concentration.

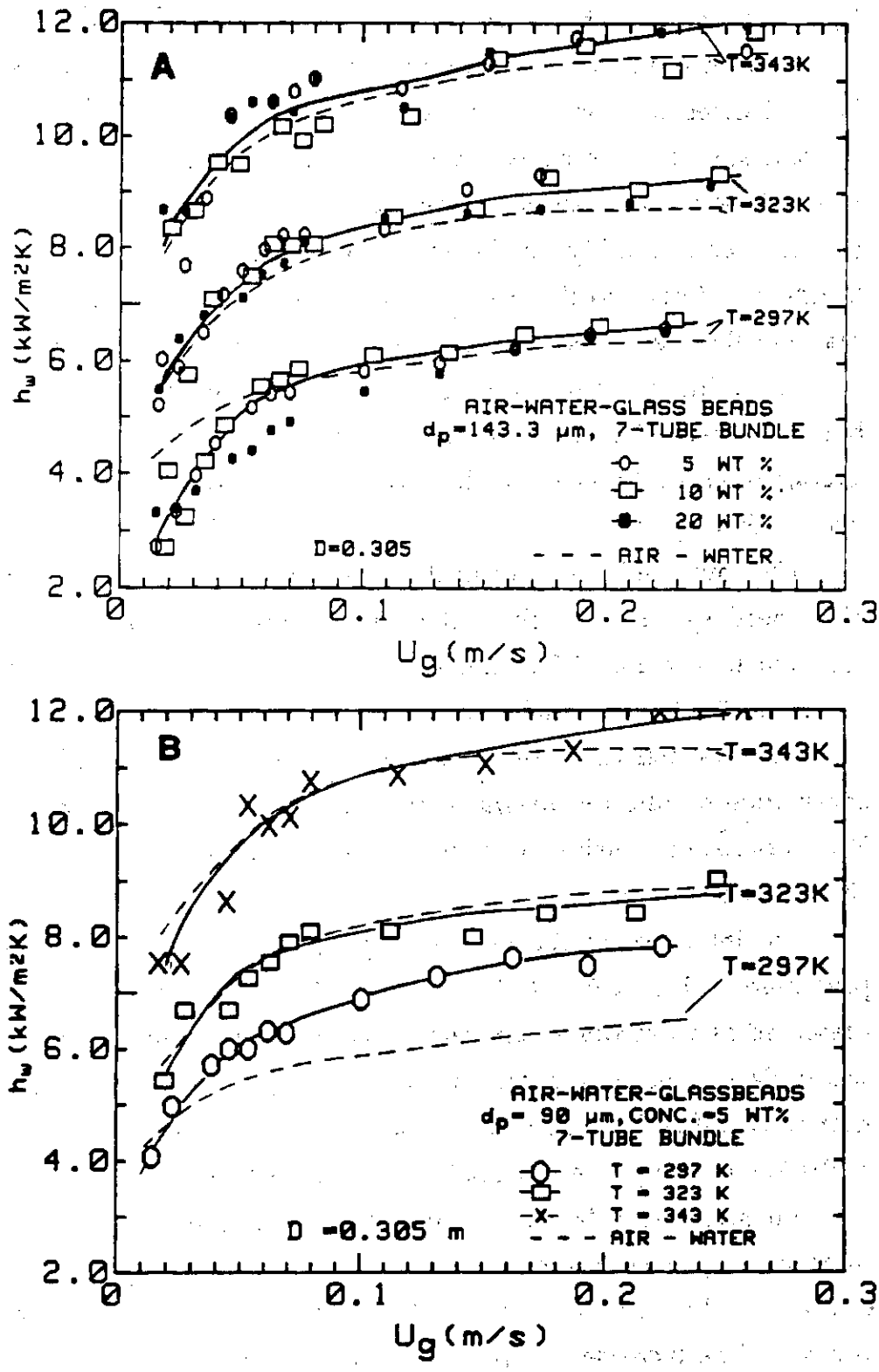

Fig. 4.69. Dependence of heat transfer coefficient on air velocity, temperature and slurry concentration for powders of mean diameter (A) 143.3μm, (B) 90 μm, (C) 50μm, and (D) 50-143 μm.

by the data of air-water-glass bead system, both qualitatively and quantitatively.

Figures 4.69B and 4.69C present the heat-transfer data for smaller size glass bead slurries of average diameters 90 and 50 μm respectively. The slurry concentration in both cases is 5 weight percent. The differences in the two- and three-phase values seem to be appreciable at room temperature. The differences decrease considerably as the temperature increases. All other characteristic trends are similar to those as seen in the case of Fig. 4.69A. Figure 4.69D is a graph of the heat-transfer coefficient values at each temperature, averaged for the various solids concentrations (including zero) and particle sizes. The vertical bars represent the range of maximum variation. We have employed these averaged values to assess various theoretical models and correlations discussed later in this report.

The smoothed values of heat-transfer coefficient for air-water and air-water-glass bead system at each of the temperatures, as a function air velocity, are reported in Table 4.35 for slurries of three different average particle sizes. The values for 143.3 μm particles are averaged for all the three slurry concentrations

Heat transfer coefficients measured at probe locations 1 and 3 in the thirty-seven tube bundle for air-water-glass bead system are reported in this section. The parameters considered include gas velocity, temperature, particle size and slurry concentration.

The influence of the operating parameters on heat transfer coefficient is presented in Fig. 4.70 - 4.72. In Fig. 4.72A the data for air-water system are presented as a function of air velocity at three temperatures. Similar data for air-water-glass gean system are displayed in Fig. 4.72B. The values for probe 3, shown by unfilled symbols, are always greater than the corresponding values for probe 1, shown by filled symbols. The magnitude of the the difference between the two sets depends on the operating conditions. The filled symbols are smoothed by a continuous curve while broken curves smooth the unfilled symbols. The heat transfer coefficient values in all cases increase with air velocity. The increase is rapid in the beginning but the same slows down with increase in air velocity and the heat transfer coefficient approaches to almost constant values at higher air velocities. The heat transfer coefficient increases for a particular system and operating conditions as the temperature is increased. In

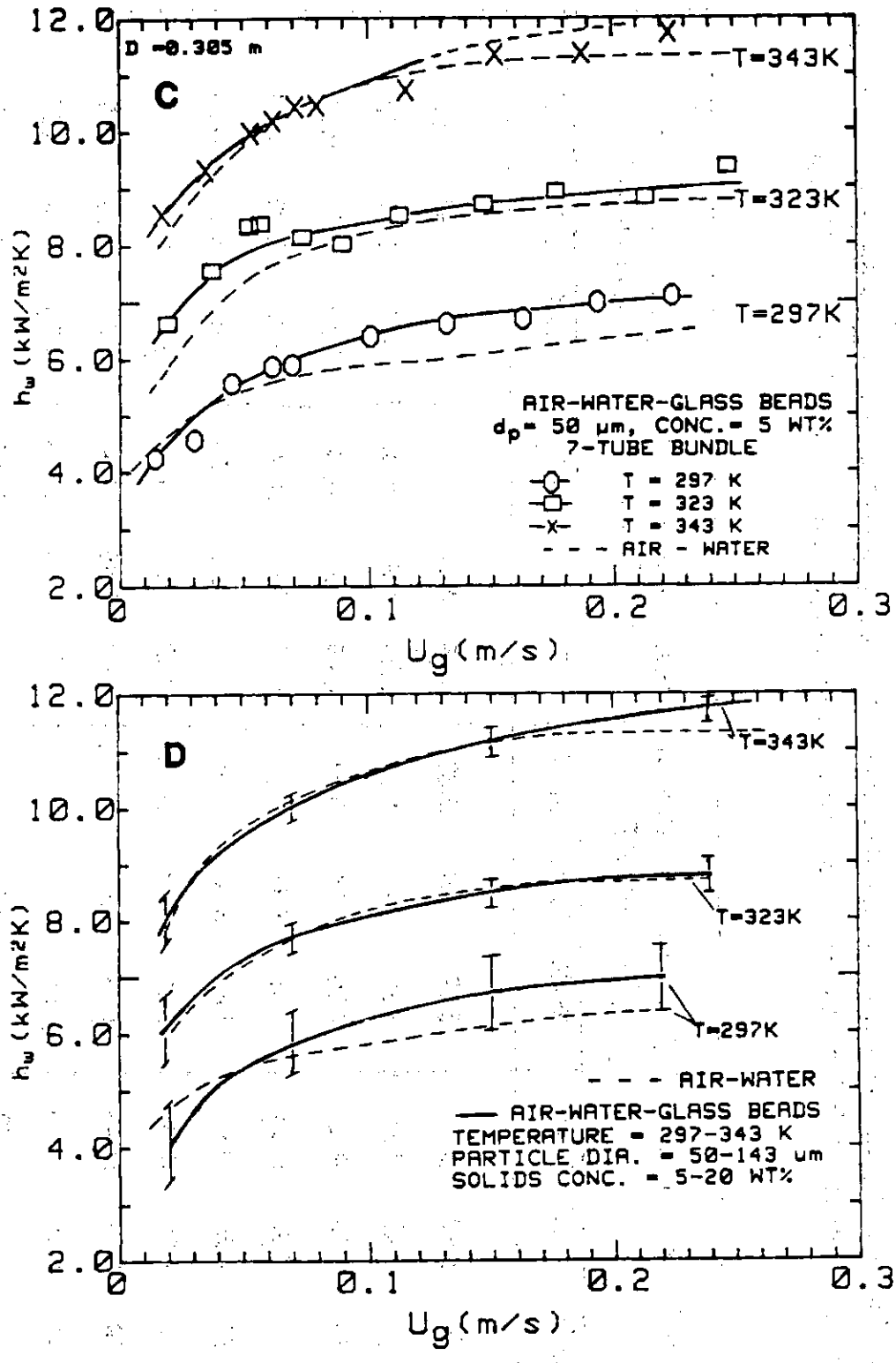

Fig. 4.69. Dependence of heat transfer coefficient on air velocity, temperature and slurry concentration for powders of mean diameter (A) 143.3μm, (B) 90 μm, (C) 50μm, and (D) 50-143 μm.

Table 4.35. Smoothed h_W (kW/m^2K) values for air-water and air-water-glass bead systems at different temperature levels. Column diameter: 0.305 m, Internal: Seven-tube bundle, Particle diameters: 50, 90 and 143.3 μm.

U_g	Solids conc. = 0 wt.%			Solids conc. = 5-20 wt% (d_p = 143.3 μm)			Solids conc. = 5 wt.% (d_p = 90 μm)			Solids conc. = 5 wt.% (d_p = 50 μm)		
(m/s)	297K	323K	343K	297K	323K	343K	297K	323K	343K	297K	323K	343K
0.02	4.60	5.90	8.01	3.17	5.50	7.80	4.65	5.70	---	4.39	6.80	8.61
0.03	5.15	6.40	8.95	3.95	6.40	8.80	5.28	6.35	8.38	4.73	7.11	9.12
0.05	5.50	7.30	9.70	4.90	7.34	9.92	6.05	7.05	9.41	5.50	7.61	9.80
0.07	5.70	7.82	10.25	5.41	7.92	10.35	6.57	7.49	10.05	5.90	8.00	10.29
0.10	5.92	8.25	11.00	5.88	8.30	10.70	7.05	7.91	10.63	6.30	8.36	10.80
0.15	6.10	8.70	11.30	6.14	8.70	11.28	7.49	8.29	11.13	6.81	8.69	11.48
0.20	6.30	9.02	11.45	6.48	8.92	11.52	7.70	8.45	11.48	7.00	8.85	11.70
0.22	6.41	9.15	11.60	6.56	---	---	7.75	8.49	11.58	7.05	8.90	11.75
0.24	---	9.30	11.62	---	9.10	11.65	---	8.49	11.67	---	8.90	11.75
0.26	---	---	11.63	---	---	11.68	---	---	11.70	---	---	11.80

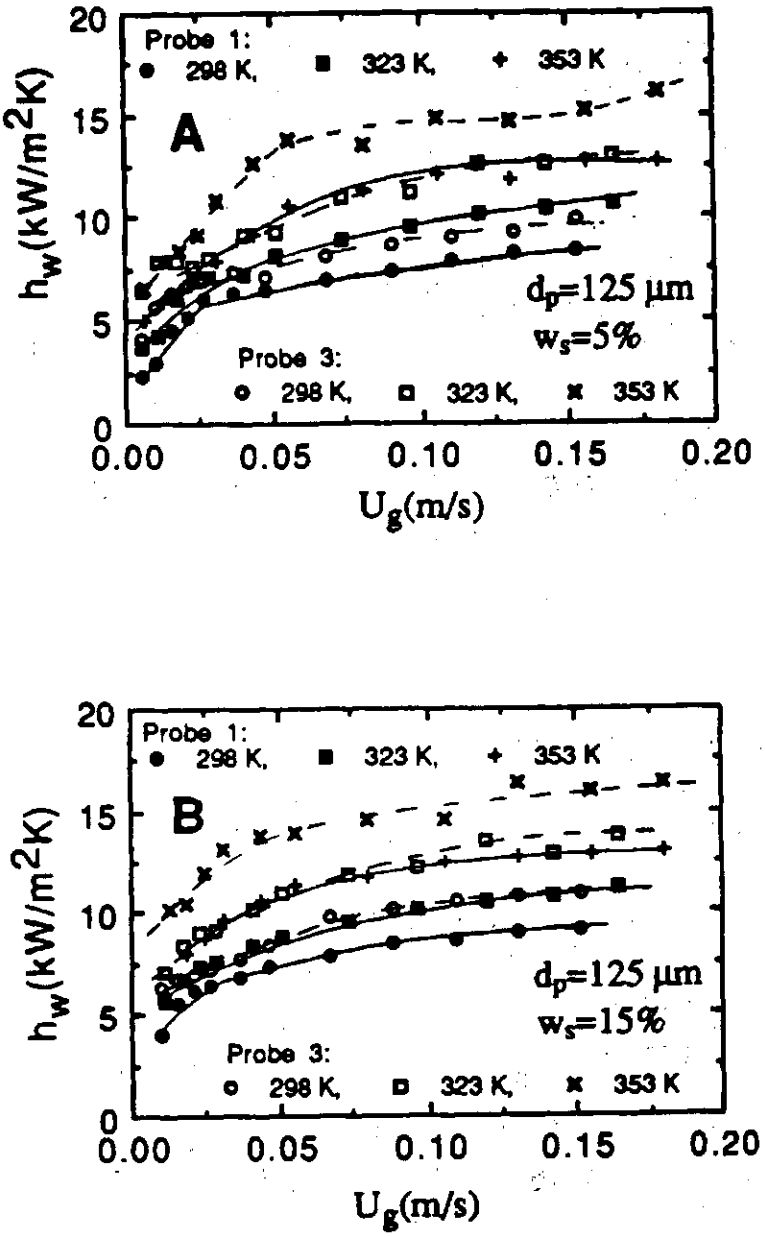

Fig. 4.70. Variation of heat transfer coefficient for the air-water-glass bead system with superficial air velocity and temperature for heat transfer probes 1 and 3 and slurries of 125 µm particles at two concentrations.

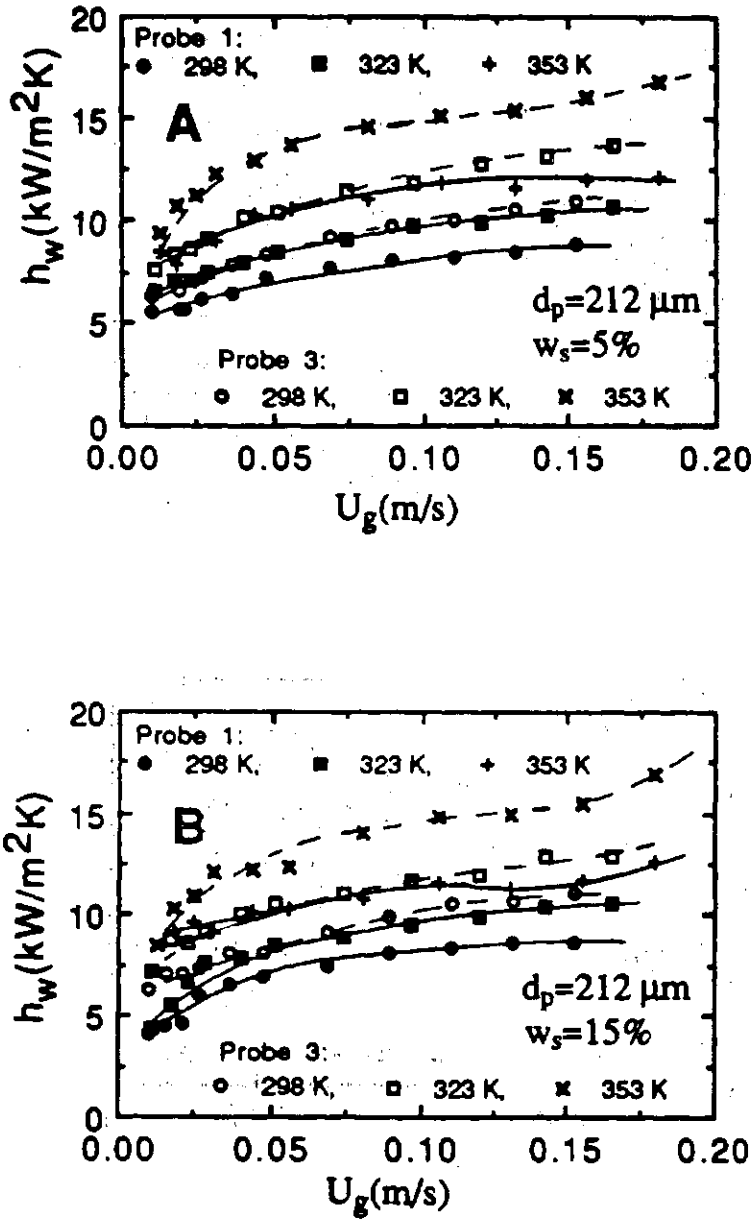

Fig. 4.71. Variation of heat transfer coefficient for the air-water-glass bead system with superficial air velocity and temperature for heat transfer probes 1 and 3 and slurries of 212 µm particles at two concentrations.

Table 4.34. Smoothed h_W (kW/m^2K) values for air-water and air-water-silica sand systems at different temperature levels. Column diameter: 0.305 m, Internal: Seven-tube bundle, Particle diameter: 65.0 μm.

U_g (m/s)	Heat transfer coefficient, h_w (kW/m^2K)					
	Solids conc. = 5 wt % (d_p = 65 μm)			Solids conc. = 10 wt % (d_p = 65 μm)		
	297K	323K	343K	297K	323K	343K
0.02	4.87	-	9.00	4.72	6.10	9.11
0.03	5.19	6.71	9.40	5.00	6.65	10.00
0.05	5.50	7.15	10.45	5.38	7.55	11.50
0.07	5.80	7.67	11.00	5.52	8.18	12.25
0.10	6.07	8.21	11.55	5.70	8.79	12.40
0.15	6.30	8.83	11.90	6.00	9.75	-
0.20	6.48	9.20	12.10	6.41	10.32	-
0.22	6.52	9.27	12.11	6.51	10.58	-
0.25	-	9.30	12.15	-	10.80	-
0.27	-	-	12.15	-	-	-

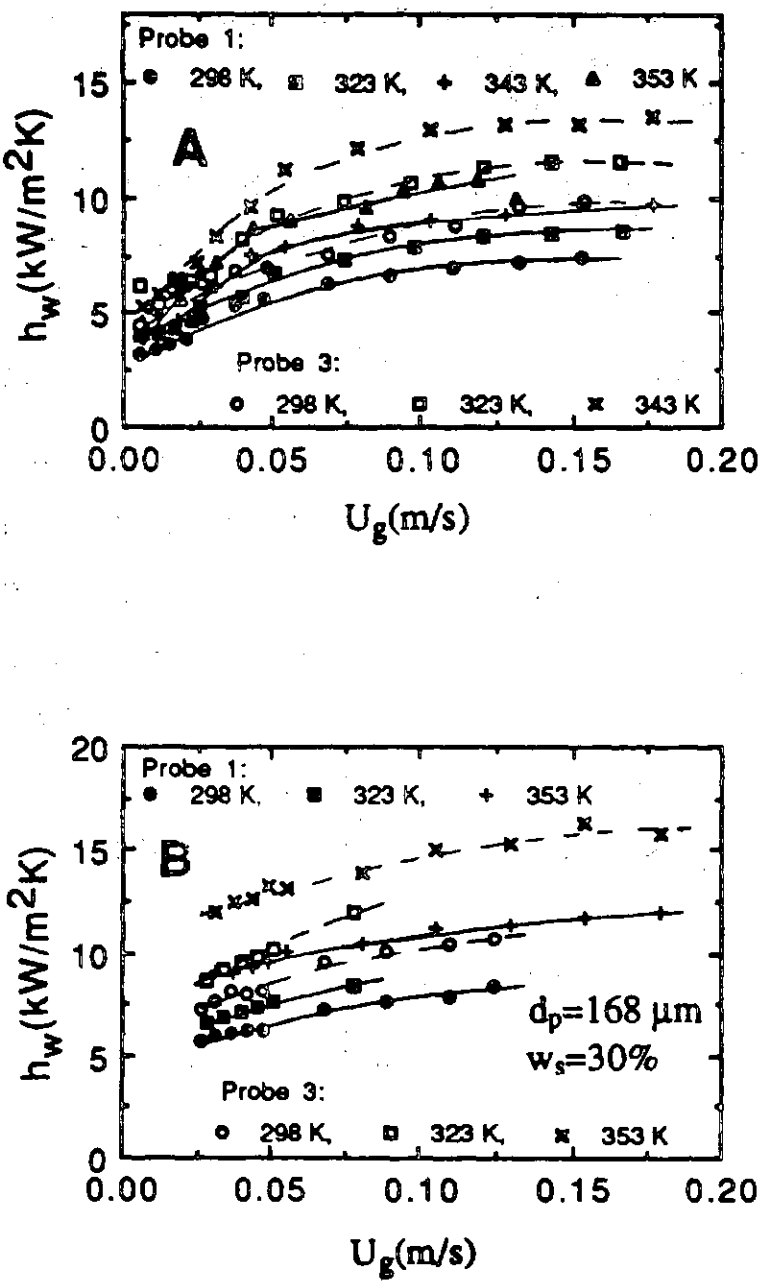

Fig. 4.72. Variation of heat transfer coefficient for (A) air-water and (B) air-water-glass bead systems with superficial air velocity and temperature for heat transfer probes 1 and 3.

further consideration of the dependence of heat transfer coefficient on operating and system parameters, data obtained from probe 3 are only considered. Smoothed h_w values for probe 3 and given in Table 4.36.

Figure 4.73 emphasizes the dependence of slurry particle diameter on heat transfer coefficient. Slurries of smaller particles (125 μm) have a slightly smaller heat transfer coefficient than for slurries of larger particles (212 μm). This difference fades out and the values are almost the same for the slurries of two particle sizes as the concentration of solids in the slurry increases from 5 to 15 weight percent. This particle dependence seems to be almost independent of temperature in the range 298 - 353K.

The influence of slurry concentration is displayed in Fig. 4.74. The dashed curve represents the average values obtained from experimental data for the air-water system. For small particle slurries (125 μm), the increase in slurry concentration results in an increase in the heat transfer coefficient values at all temperatures. This increase is more at ambient temperature and decrease with increase in temperature but then remains constant with further increase in temperature. For slurries of larger particles (212 μm), the increase in slurry concentration has only nominal effect on h_w temperatures and over the air velocity range.

4.6.6 Air-Water-Magnetite System

Heat transfer data measured at the centrally located heat transfer probe in seven-tube bundle configuration are presented for the air-water-magnetite system in Fig. 4.75. Some interesting conclusions are evident from these graphical presentation of data. First, the variations of h_w with U_g and T_c are similar to those for the air-water system. Secondly, the influence of slurry concentration on h_w is negligibly small, and values for the air-water system may be regarded approximately to be same as the air-water-magnetite system. Thirdly, the effect of slurry particle size in the range of present investigations on h_w is nominal and may be neglected. These averaged and smoothed h_w values

Table 4.36. Smoothed hw (kW/m2 K) values for air-water-glass bead system at different temperature levels. Column diameter: 0.305m, Internal: Thirty-seven tube bundle, Particle diameters: 125, 168 and 212 μm

h_w / U_g	d_p = 125 μm						d_p = 212 μm						d_p = 168 μm		
	W_s = 5%			W_s = 15%			W_s = 5%			W_s = 15%			W_s = 30%		
	298K	323K	353K	298K	323K	353K	298K	323K	353K	298K	323K	353K	298K	323K	353K
0.02	6.50	7.50	9.00	7.00	8.25	11.25	7.00	8.50	10.50	7.00	8.25	10.50	-	-	-
0.04	7.25	9.25	12.00	8.00	10.00	13.00	8.00	9.90	12.40	8.00	9.75	12.00	8.00	9.60	12.50
0.06	7.75	10.25	13.50	9.00	11.25	14.50	8.75	10.90	13.50	9.00	10.75	13.00	9.00	10.90	13.40
0.08	8.25	11.25	14.50	9.75	12.25	14.50	9.50	11.60	14.40	9.75	11.25	13.75	9.70	12.00	14.00
0.10	8.50	11.90	14.75	10.25	12.75	15.50	9.70	12.10	14.80	10.25	11.75	14.40	10.25	-	14.75
0.12	9.25	12.25	14.75	10.60	13.25	15.40	10.30	12.50	15.10	10.60	12.25	14.75	10.75	-	15.25
0.14	9.75	12.75	15.00	10.90	13.50	15.75	10.70	13.25	15.50	10.90	12.50	15.10	-	-	15.60
0.16	-	13.00	15.25	-	13.60	16.00	-	13.50	16.00	-	12.90	15.50	-	-	15.80
0.18	-	-	16.00	-	-	16.25	-	-	16.60	-	-	16.50	-	-	16.00

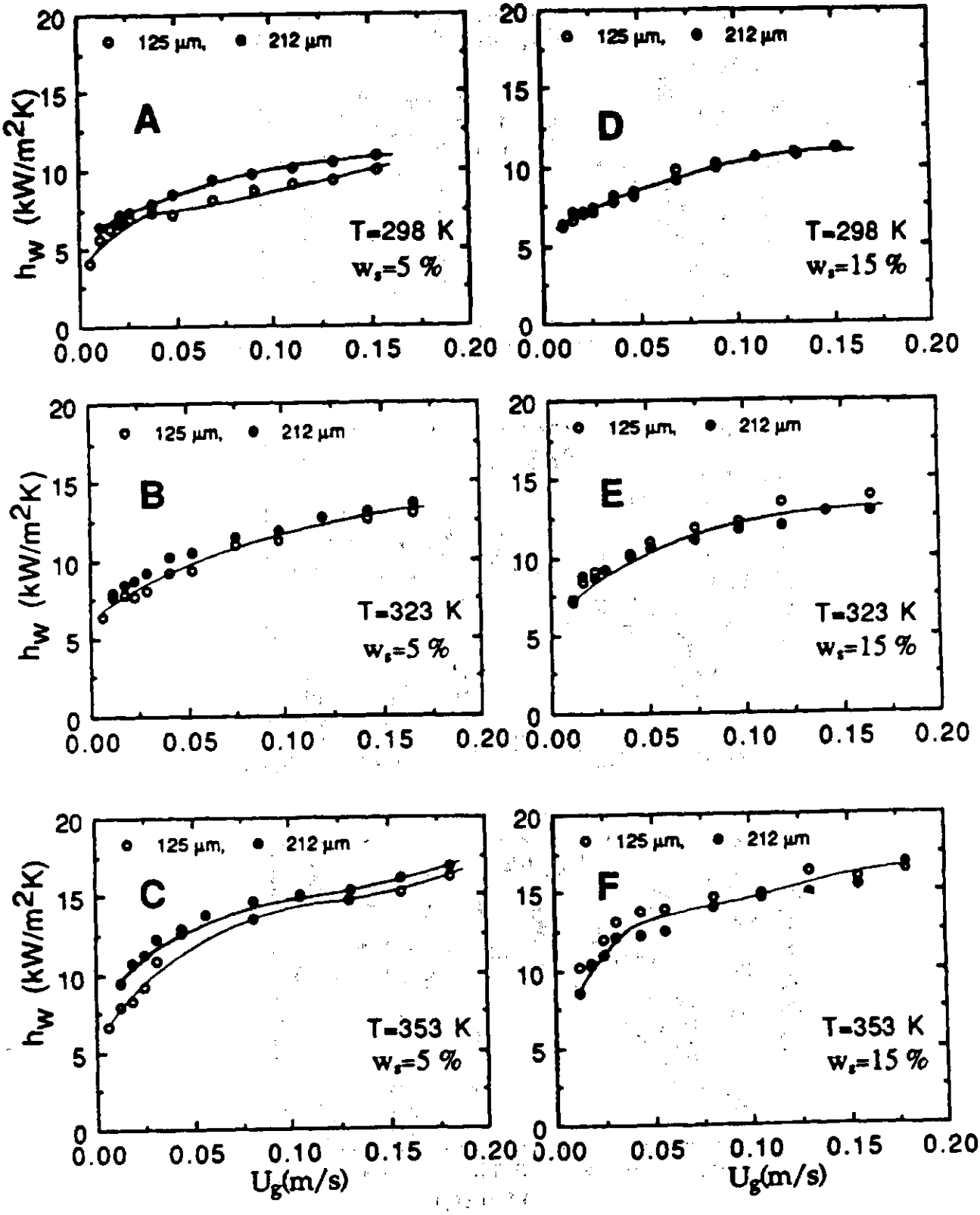

Fig. 4.73. Effect of particle diameter on heat transfer coefficient at different temperatures for two slurry concentrations and heat transfer probe 3.

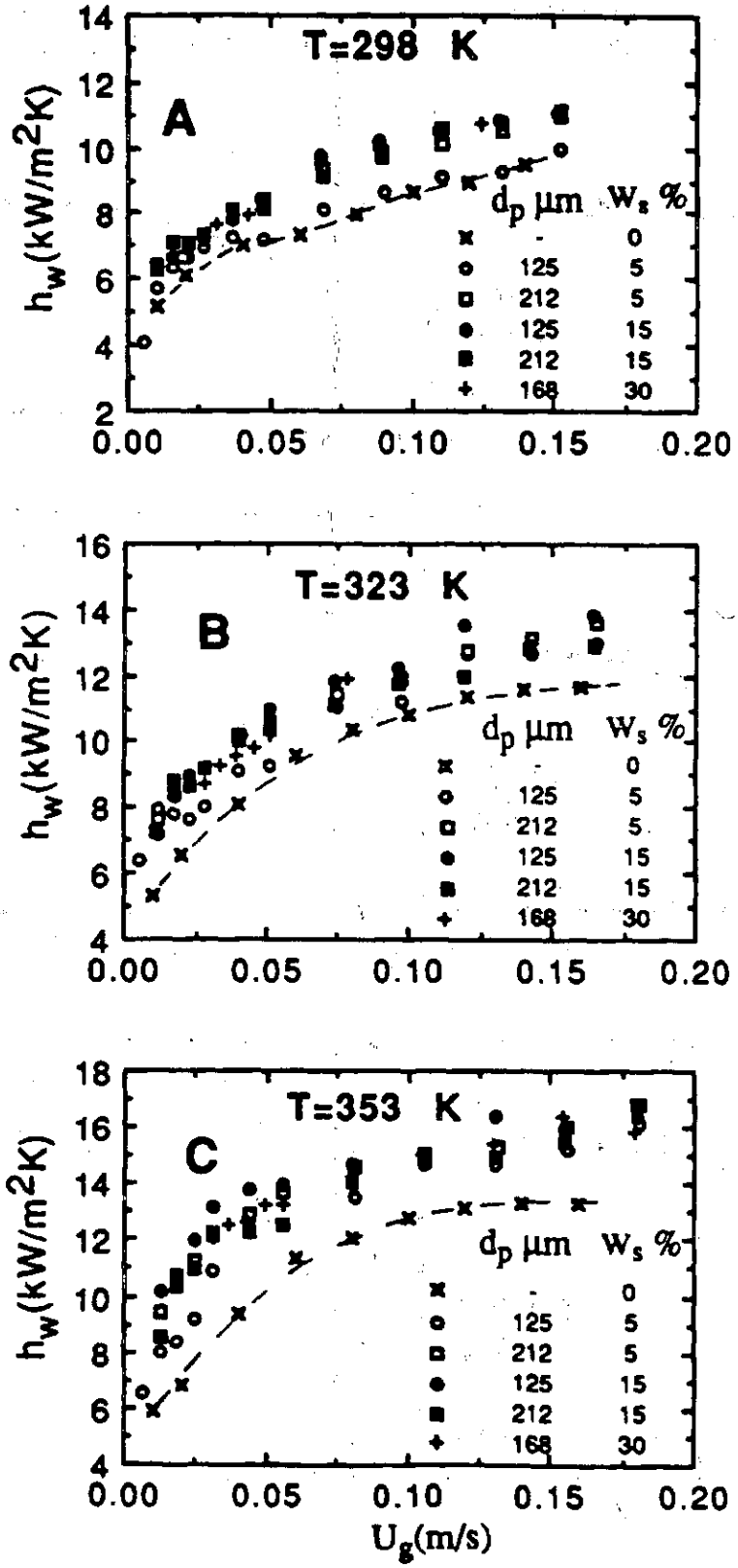

Fig. 4.74. Effect of slurry concentrations on heat transfer coefficient at different temperatures and slurry particle sizes for heat transfer probe 3.

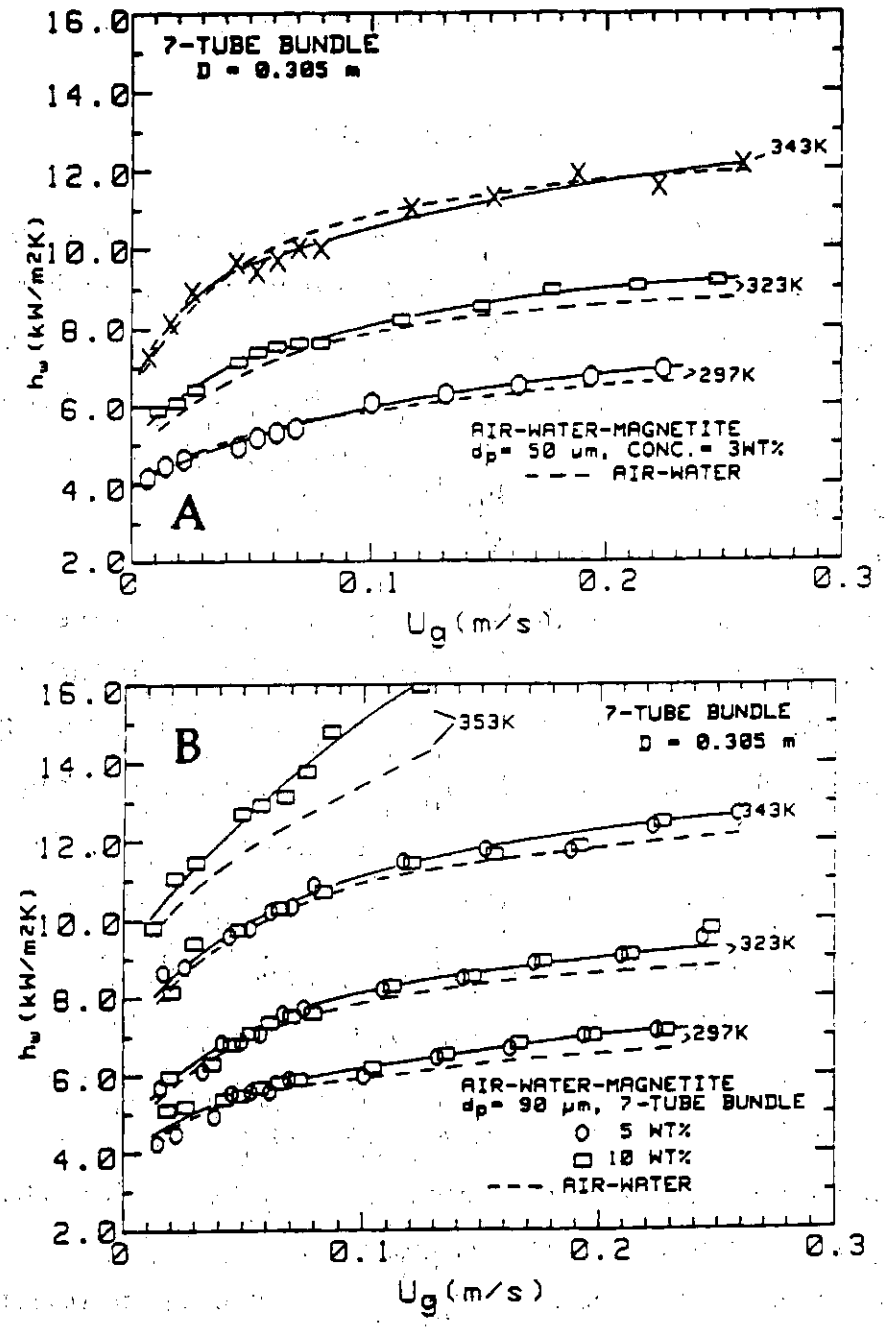

Fig. 4.75. Dependence of heat transfer coefficient on air velocity, temperature, particle size and slurry concentration. (A) 50 μm and 3 wt %; (B) 90 μm, 5 and 10 wt %.

are reported in Table 4.37 as a function of temperature and air velocity.

4.6.7 Nitrogen-Therminol-Magnetite System

From Figs. 4.76 - 4.78, it is clear that the heat transfer coefficient measured at lower vertical positions (P1 and P2) are greater than at higher vertical positions (P3 and P4). In the nonfoaming regime (Figs. 4.76 a - c, 4.77 a - c, 4.78 a - c), h_w is not dependent on the radial position. Probes 1 and 2, and probes 3 and 4 give identical results. On the other hand, in the foaming regime (Figs. 4.76 d - f, 4.77 d - f and 4.78 d - f) there is an involved dependence. h_w increases with the increase in radial position and this increase is less as the vertical height increases. A slightly different trend exhibited in Fig. 4.78f is due to the unique behavior of foaming observed at 523K as mentioned before. To further investigate the dependence of h_w on different parameters, data corresponding to probe 1 only are considered and for most cases this is the upper bound for h_w.

In Fig. 4.79, the heat transfer data are displayed to highlight the dependence of h_w on solids concentration and nitrogen velocity at different temperatures. In each case h_w increases monotonically with U_g, the increase being rapid at lower velocities and less rapidly as U_g increases. It appears that h_w increase with increase in solids concentration, the increase is not always quite explicit and sometimes the trend seems to reverse for values of w_s below 30 percent. The data corresponding to 40 percent are in almost all cases distinctly greater than the corresponding values at lower concentrations.

In Fig. 4.80, the experimental heat transfer data are presented to highlight the influence of temperature on heat transfer coefficient. In each case, we see an unambiguous increase in the values of h_w with increase in temperature at the same solids concentration and gas velocity. Smoothed h_w values for different probe locations are given in Table 4.33.

Table 4.37. Smoothed h_W (kW/m^2K) values for air-water and air-water-magnetite systems at different temperature levels. Column diameter: 0.305 m, Internal: Seven-tube bundle. Particle diameters: 50 and 90 μm. Solids concentrations: 3, 5 and 10 wt%.

U_g	Air-Water System			Air-Water-Magnetite System		
m/s	297K	313K	343K	297K	323K	343K
0.02	0.067	0.046	0.035	0.052	0.054	0.054
0.03	0.100	0.063	0.051	0.100	0.083	0.072
0.05	0.152	0.101	0.080	0.180	0.132	0.105
0.07	0.187	0.132	0.108	0.250	0.168	0.132
0.10	0.233	0.173	0.142	0.280	0.185	0.157
0.15	0.243	0.205	0.190	0.265	0.220	0.197
0.20	0.267	0.240	0.218	0.280	0.255	0.230
0.22	0.280	0.255	0.232	0.295	0.272	0.245
0.24	-	0.270	0.245	-	0.280	0.260
0.26	-	-	0.263	-	0.290	0.270

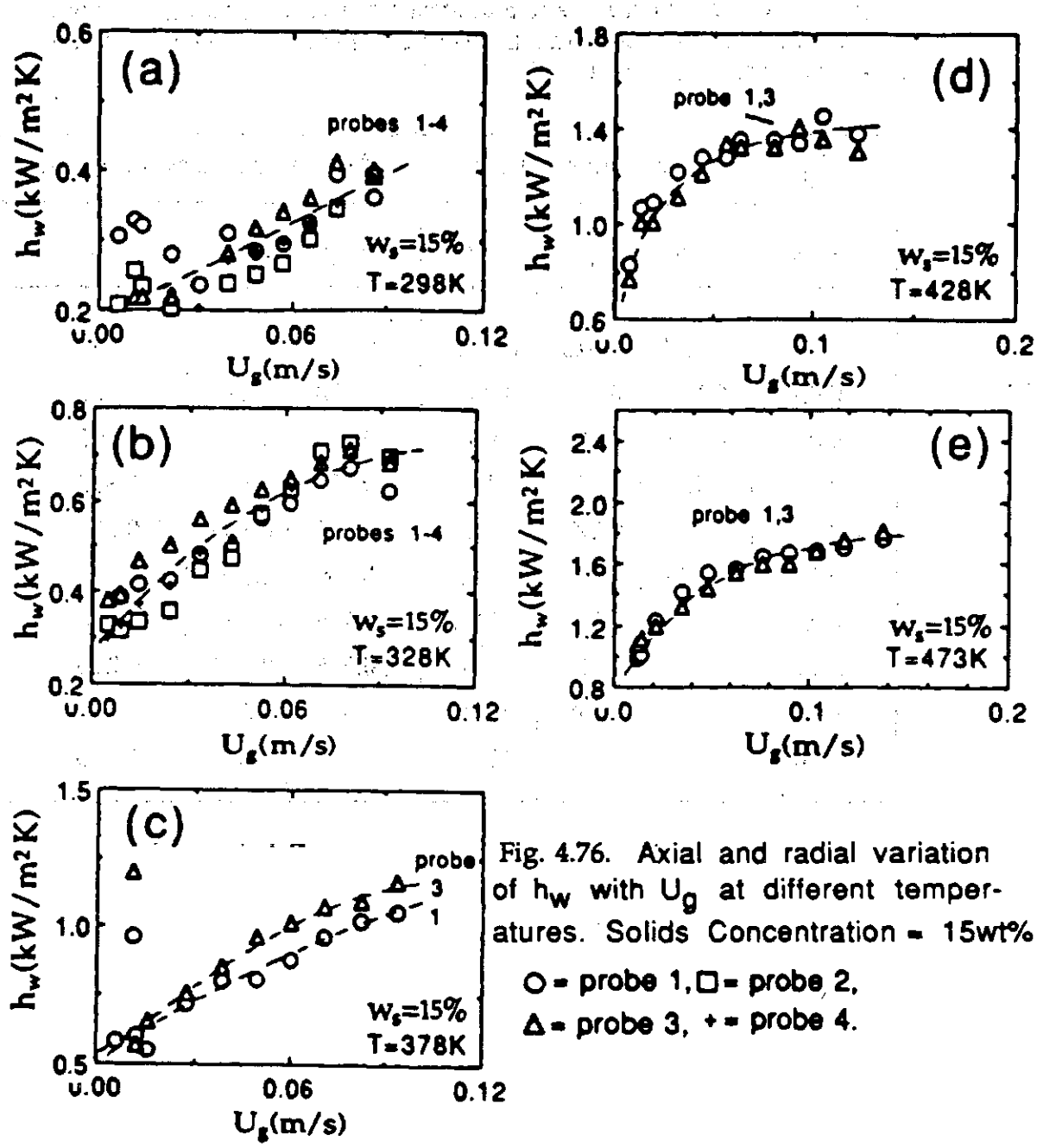

Fig. 4.76. Axial and radial variation of h_w with U_g at different temperatures. Solids Concentration = 15wt%.

○ = probe 1, □ = probe 2,
△ = probe 3, + = probe 4.

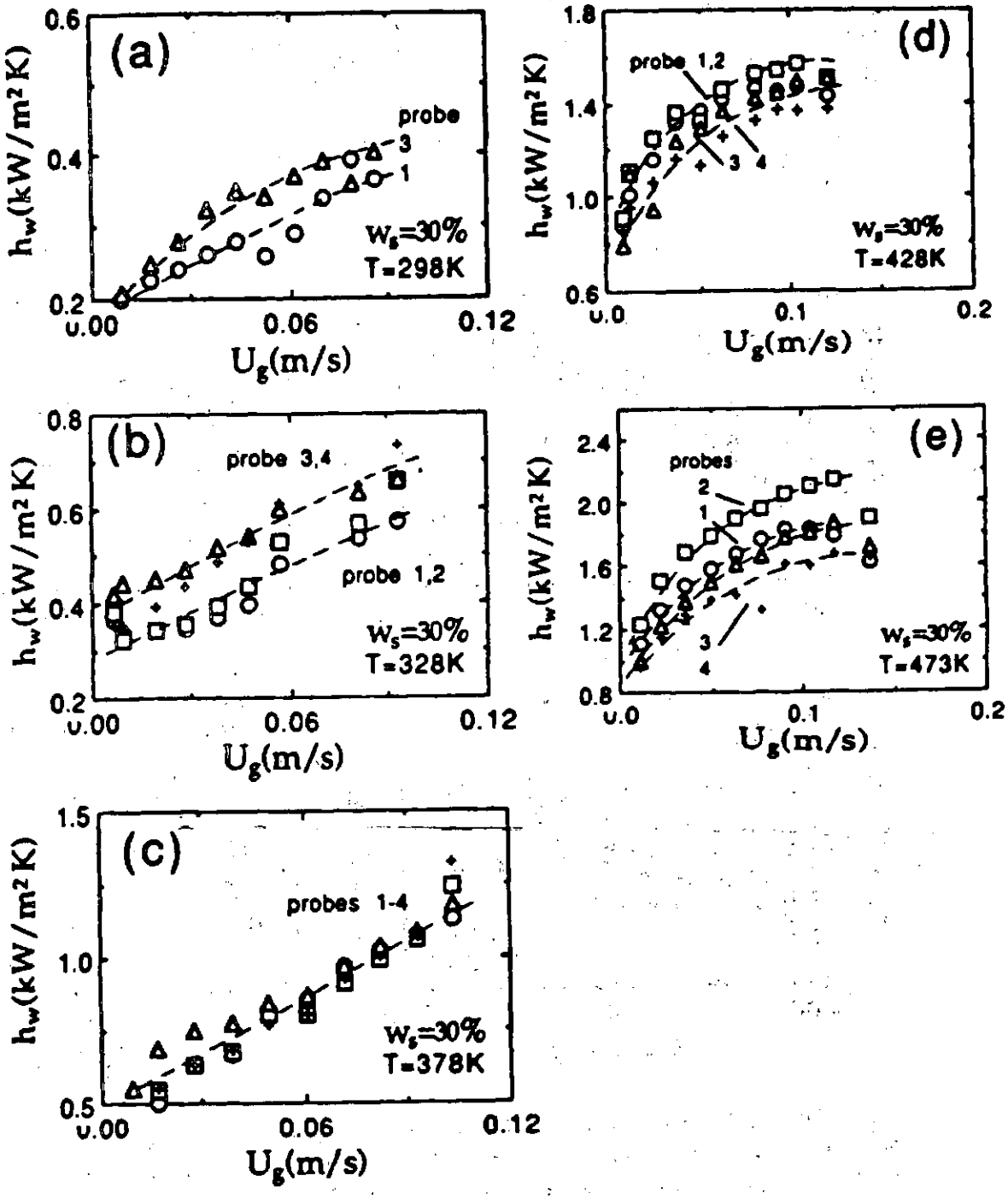

Fig. 4.77. Axial and radial variation of h_W with U_g at different temperatures. Solids concentration = 30 wt %.

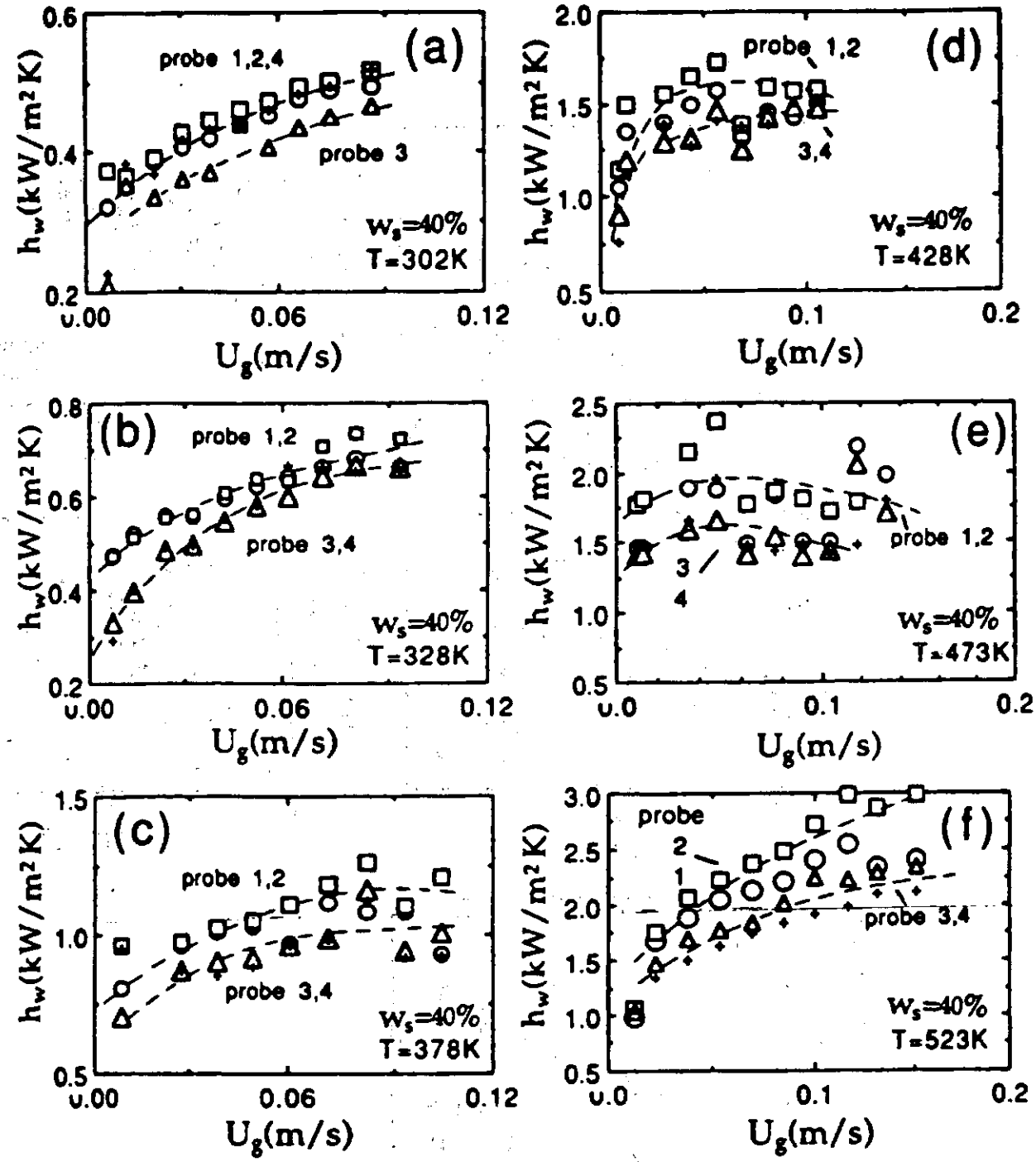

Fig. 4.78. Axial and radial variation of heat transfer coefficient with nitrogen velocity at different temperatures. Solids conc. = 40 weight percent. ○ = probe 1, □ = probe 2, △ = probe 3, + = probe 4.

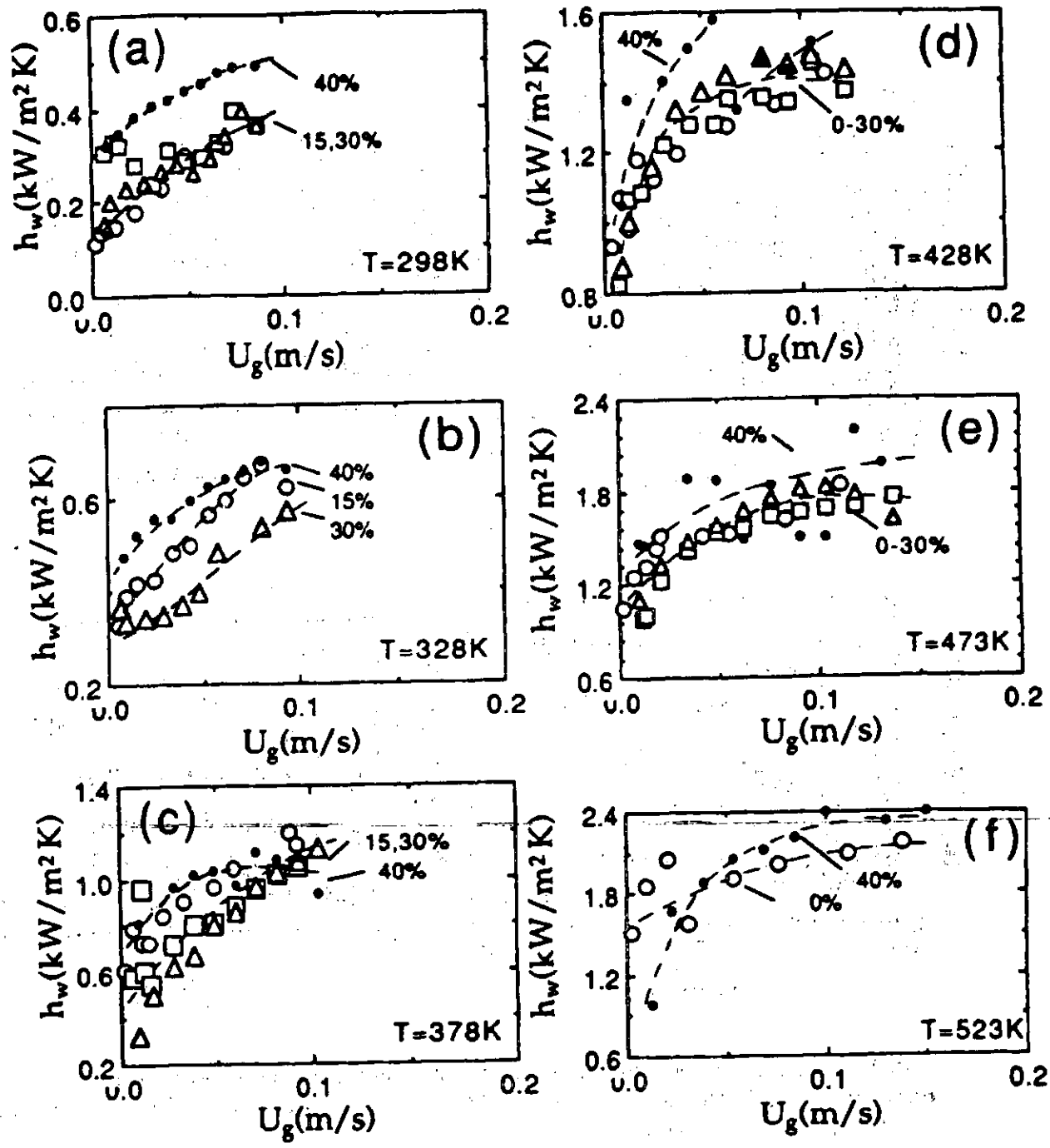

Fig. 4.79. Variation of heat transfer coefficient (probe 1) with nitrogen velocity and solids concentration at different temperatures. ○ = 0 wt%, □ = 15 wt%, △ =30 wt%, ● = 40 wt%.

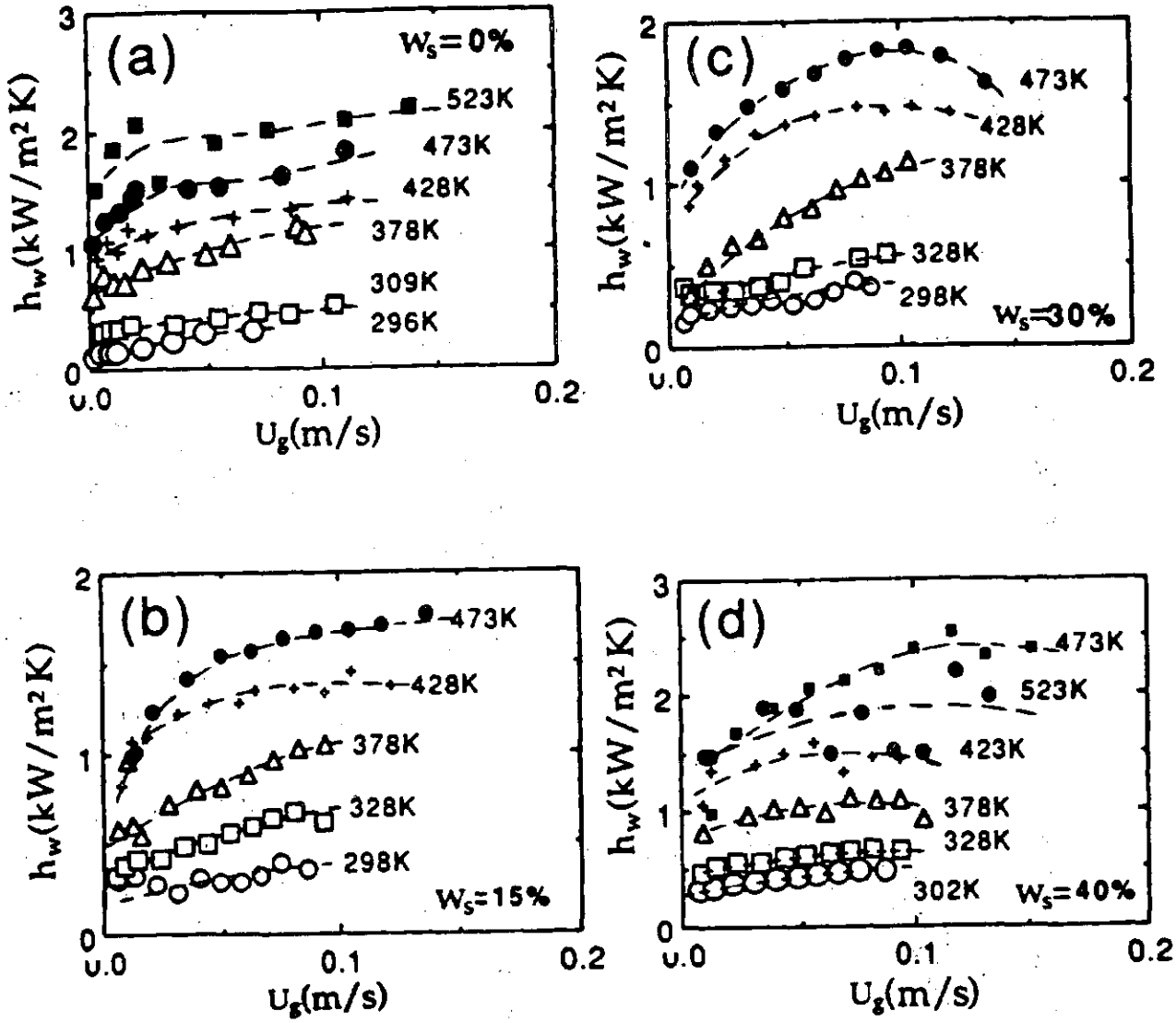

Fig. 4.80. Effect of temperature on heat transfer coefficient at different solids concentrations in the slurry. ○ = 298K, □ = 328K, △ = 378K, + = 428K, ● = 473K, ■ = 523K.

•U.S. GOVERNMENT PRINTING OFFICE: 1991 -548-138/40054